ANALYSIS OF SEISMOGRAMS FROM A DOWNHOLE ARRAY IN SEDIMENTS NEAR SAN FRANCISCO BAY

by

William B. Joyner, Richard E. Warrick, and Adolph A. Oliver III

U.S. Geological Survey

OPEN FILE REPORT

76-296

This page intentionally left blank

ABSTRACT

A four-level downhole array of three-component instruments was established on the southwest shore of San Francisco Bay to monitor the effect of the sediments on low-amplitude seismic ground motion. The deepest instrument is at a depth of 186 meters, two meters below the top of the Franciscan bedrock. Earthquake data from regional distances (29 km $\leq \Delta \leq$ 485 km) over a wide range of azimuths are compared with the predictions of a simple plane-layered model with material properties independently determined. Spectral ratios between the surface and bedrock computed for the one horizontal component of motion that was analyzed agree rather well with the model predictions; the model predicts the frequencies of the first three peaks within 10 percent in most cases and the height of the peaks within 50 percent in most cases. Surface time histories computed from the theoretical model predict the time variations of amplitude and frequency content reasonably well, but correlations of individual cycles cannot be made between observed and predicted traces.

INTRODUCTION

In the summer of 1970, the U.S. Geological Survey established a four-level downhole array of three-component seismometers on the southwest shore of San Francisco Bay to monitor the effect of the sediments on seismic ground motion. The deepest instrument is at a depth of 186 meters, two meters below the top of the Franciscan bedrock.

Earlier work in the San Francisco Bay area by Borcherdt (1970) showed marked amplitude variations in surface recordings of distant nuclear explosions. Those variations were consistently related to the geology of the recording site in a way that paralleled the relationship between geology and 1906 earthquake intensities as reported by Wood (1908).

The effect of local geology on earthquake ground motion is a controversial subject that has generated a rather large literature. Recent discussions the subject from different points of view are given by Seed and Schnabel (1972), Hudson (1972), Newmark and others (1972), Murphy, Davis, and Weaver (1971), Campbell and Duke (1974), and Dobry, Whitman, and Roesset (1971). In this paper we present the results of recording a number of earthquakes at the downhole array and compare those results with the predictions of a simple plane-layered model based on measurements of the dynamic properties of the material at the site (Warrick, 1974).

All of our recordings are of small motions, below the level of perceptibility. The maximum particle velocity is approximately 3 mm/sec and the maximum strain in the soil is of the order of 10^{-5}. For strains that small, the material behavior is essentially linear. Our results are therefore not applicable to strong ground motion without modifications to allow for the strain dependence of the dynamic properties of the soft sediments.

Shima (1962) presented an analysis of data from downhole arrays extending to a depth of 21 meters at Tokyo Station. These data were analyzed further by Dobry, Whitman, and Roesset (1971). Data from a 31-meter downhole array in Union Bay, Seattle, Washington, were analyzed by Seed and Idriss (1970), Tsai and Housner (1970), and Dobry, Whitman, and Roesset (1971). A number of downhole arrays in soil have been established recently in Japan as described by S. Ibukiyama, E. Kuribayashi, and T. Iwasaki at the Fourth Joint Meeting of the U.S.-Japan Panel on Wind and Seismic Effects in May 1972 and by S. Hayashi and H. Tsuchida at the Sixth Joint Meeting of the Panel in May 1974.

THE SITE

The location of the downhole array is shown in Figure 1. The geologic section at the site (Figure 2) consists of 11 meters of bay mud underlain by alluvium, which in turn is underlain by Franciscan graywacke at a depth of 184 meters. Seismometers are located on the surface, just below the base of the bay mud at a depth of 12 meters, in the alluvium at a depth of 40 meters, and in the Franciscan bedrock at a depth of 186 meters.

The bay mud is a Holocene estuarine deposit, predominantly soft clay and silty clay, generally containing more than 50 percent water by weight. The alluvium, which may be as old as Pliocene at the base and as young as Holocene at the top, consists predominantly of clay with interbedded sand and gravel. The clay within the alluvium is generally stiffer than the bay mud with a lower water content and a greater degree of preconsolidation. The layer of alluvium occupies a northwest-southeast trending trough in the middle of which lies San Francisco Bay. Perpendicular to the axis of the trough, the layer extends 9 km to the southwest and 15 km to the northeast of the site. It is bounded on both sides by hills in which Tertiary and pre-Tertiary bedrock is exposed. (Lajoie and Helley, 1975; Borcherdt and others, 1975; Warrick, 1974; Schlocker, 1970; Treasher, 1963; H. W. Olsen, unpublished data.)

INSTRUMENTATION AND DATA ANALYSIS

Each of the instrument packages below the surface was installed at the bottom of a separate, uncased drill hole. The packages at the surface and at 12 meters were oriented to the cardinal directions by mechanical means. The orientation of the packages at the two deeper levels could not be controlled, but, after the instruments were emplaced, their orientation was determined to within about 5° by recording the direction of first motion of seismic waves from small explosive charges set off at known azimuths.

Each instrument package consists of three mutually perpendicular velocity transducers (Mark Products L-1), one vertical and two horizontal. Nominal resonant frequency is 4.5 Hz, sensitivity 0.3 volts/cm/sec, and damping approximately 0.6 critical. The output of the seismometers is amplified, filtered by a 37 Hz or a 9 Hz low pass filter, and continuously recorded on FM magnetic tape, along with time signals from the National Bureau of Standards station WWVB. A 3 Hz sinusoidal calibration signal of known voltage applied to the amplifier input is recorded at the beginning and end of each tape reel.

Preliminary evaluation of recorded events is made using playbacks from a 14-channel oscillograph. Selected events are digitized for further analysis. Generally, the digitization rate is 50 samples per second. When an event is digitized, a noise sample of equal length immediately preceding the event is also digitized as well as the calibration signal from the beginning of the tape reel. The first step in digital analysis of the data is determination of the amplitude of the calibration signal and the adjustment of all data channels to a common gain level. The data from the horizontal seismometers are then transformed to a common coordinate system parallel to the cardinal directions.

The earthquakes analyzed in this report are listed in Table 1 along with distance and azimuth of the epicenter from the site of the downhole array. The origin time, location, and magnitude for the San Fernando earthquake were taken from Allen and others (1971) and for the Gordo Escarpment earthquake from the Berkeley Seismographic Bulletin (Cloud and Qamar, 1972). For all of the other events, magnitudes were taken from the Berkeley Bulletin (Adams and Gopalakrishnan, 1971; Cloud and Qamar, 1972; Cloud and others, 1972, 1974a, 1974b), and the location and origin times were taken from the U.S. Geological Survey's catalog of earthquakes in central California (Lee and others, 1972a, 1972b; Wesson and others, 1973, 1974a, 1974b).

Figure 3 is an example of a seismogram produced by the preliminary stages of processing for the Anzar earthquake, a local event of magnitude 3.1 and epicentral distance 79 km. Figure 4 is the seismogram for the San Fernando earthquake of 1971 (magnitude 6.6, distance 485 km). The frequency content of the two events is very different (note the difference in time scale), and the pattern of response is correspondingly different. For the local earthquake (Figure 3), horizontal ground motion is significantly amplified relative to the bedrock level only at the surface instruments. For the San Fernando earthquake, significant amplification of horizontal motion occurs at all instrumented levels within the soil column.

In general, the character of the seismograms is affected significantly by the nature and distance of the source and the response of the instruments as well as the response of the site.

In an attempt to isolate the response characteristics of the site from the effects of the source and the instrument response, we compare the motion at different levels using ratios of Fourier amplitude spectra (Borcherdt, 1970). Before a spectrum is computed, the seismogram is multiplied by a window to minimize spectral leakage. The window used is flat in the central portion and has a cosine half-bell taper occupying 10 percent of the total window length at each end (Kanasewich, 1973, p. 93-94). The complex Fourier spectrum is then calculated using the Fast Fourier Transform program HARM from the IBM Scientific Subroutine Package. The square modulus of the spectrum is smoothed using a symmetrical 15-point triangular window. After smoothing, the square root is taken to give a smoothed modulus from which ratios are computed. In plotting the spectral ratio between different levels as a function of frequency, the spectral amplitudes of signal and noise are checked at both levels for each frequency. The point is plotted only if the ratio of signal amplitude to noise amplitude is at least two for both levels.

The minimum record length used in the analysis is 41 seconds, which gives a frequency resolution, after smoothing, of about 0.2 Hz. Except as specifically noted, the entire seismogram is used to obtain the spectrum.

The use of spectral ratios to remove the effects of source and instrument characteristics depends upon similarity in instrument response. The relative response of the instruments was tested *in situ*; the tests and results are described in the Appendix. The north-south instruments performed satisfactorily, but the east-west surface instrument showed anomalous response below 0.5 Hz. For that reason analysis is limited to the north-south component.

THEORETICAL MODEL

We compare the observed response at the site of the downhole array with a simplified theoretical model comprised of a system of horizontal, viscoelastic, soil layers bounded above by the free surface and below by a semi-infinite elastic medium. The seismic excitation is represented by a homogeneous SH wave incident at arbitrary angle in the underlying medium. Horizontally layered soil models have been widely used for predicting seismic response (Idriss and Seed, 1968a; Schnabel, Seed, and Lysmer, 1972). There is some disagreement concerning the range of applicability of this kind of model (Hudson, 1972; Newmark and others, 1972), and we desired to see how well such a model would predict the response we observed for a variety of earthquake sources at low strain levels.

Kanai (1952) solved the plane-layer problem for the case of a vertically incident SH wave in the underlying elastic medium and three horizontal soil layers with viscoelasticity of the Voigt type. Matthiesen and others (1964) adapted Kanai's solution to machine computation and extended it to an arbitrary number of layers. We use the same approach, extended to general linear viscoelastic behavior for the layers by the matrix methods of Haskell (1953, 1960), and extended to the case where the input wave in the underlying medium has arbitrary angle of incidence. A more detailed description of our procedure is given elsewhere (Joyner and Chen, 1975).

(there are no pages 10 or 11)

If the density ρ_n and the ~~complex~~ modulus μ_n are specified for each layer along with the density and modulus of the underlying medium, we can compute the response for any incident motion. For viscoelastic layers the modulus is complex and ~~The complex modulus~~ can be written in terms of real numbers as

$$\mu_n = \mu_{Rn}(1 + i/Q_n) \ .$$

Values of μ_{Rn} were obtained from measurements of shear wave velocity and values of Q_n from measurements of shear wave attenuation using the simple relationships valid under low-loss conditions as described in the following section. It was assumed that μ_{Rn} and Q_n do not depend on frequency.

For a linear medium, μ_{Rn} and Q_n could not be independent of frequency over the entire frequency band from zero to infinity without violating causality (Futterman, 1962). Considering the limited band-width of our data, however, we believe that the assumption of frequency-independent μ_{Rn} and Q_n is adequate.

DETERMINATION OF MATERIAL PROPERTIES

Our basic purpose is to see how well the observed spectral ratios are predicted by a theoretical model whose properties have been determined from independent data, rather than devising a theoretical model to fit the observed data. For assigning physical properties, the section above the bedrock interface was divided into two parts: "typical bay mud" between the surface and 8 meters depth and "alluvium" from 8 meters to bedrock. The material between 8 and 11 meters properly belongs to the bay mud unit, but data on samples obtained at the site (H. W. Olsen, unpublished data) indicate that, as far as density and shear modulus are concerned, that material is more like the alluvium than it is like the typical bay mud.

A bulk density of 1.7 gm/cm^3 was assigned to the material between the surface and 8 meters, based on measurements on samples obtained at the site (H. W. Olsen, unpublished data). For the material between 8 meters and bedrock a density of 2.05 gm/cm^3 was estimated from data given by Johnson, Moston, and Morris (1968) for a drill hole 14 km to the southeast in similar material. The density of the bedrock was estimated at 2.6 gm/cm^3. Control for assigning density to the material below 8 meters leaves something to be desired, particularly in the case of the bedrock, but the actual densities are not likely to differ from the estimates by enough to have an appreciable effect on the computed response.

Under the low-loss conditions the real part of the complex shear modulus for the nth layer is given by

$$\mu_{Rn} = \rho_n \, v_{sn}^2$$

where ρ_n is the density and v_{sn} the shear wave velocity in the nth layer. Data on shear velocity were obtained by downhole recording of shear waves artificially generated at the surface. Details of this work have already been reported (Warrick, 1974). The results provide a shear wave travel time for each of the three intervals separating the four instruments.

Using data from earthquake recordings we were able to obtain confirmation of the shear wave travel times derived from the artificially generated waves, as shown in Figure 5. The data are from a small local earthquake (magnitude 2.8, distance 45 km) digitized at 100 samples per second. Trace number 1 at the bottom is the autocorrelation of the north component at bedrock. Traces 2, 3, and 4 are the cross correlation of the north component at bedrock with, successively, the north components at the 40 m, 12 m, and surface levels. The upper three traces show readily identifiable peaks corresponding to the travel time from the bedrock level to each of the other levels. The travel times thus indicated agree to within 0.01 second with the data from the artificially generated shear waves. The earthquake wave did not travel vertically through the sediments, but for reasonable assumptions concerning the shear velocity of the bedrock the maximum departure from the vertical is about 10°, and the corresponding correction to the travel time is less than 0.01 second.

The interval shear velocities (Warrick, 1974) are 90 meters/sec from the surface to 12 meters, 260 meters/sec from 12 meters to 40 meters, and 380 meters/sec from 40 meters to bedrock. A higher velocity is indicated for the alluvium compared to the bay mud and an increase in velocity with depth in the alluvium. This increase of velocity with depth is to be expected from the laboratory results of Hardin and Black (1969) and Hardin and Drnevich (1972a, 1972b) showing the influence of ambient effective stress upon shear modulus. In developing a theoretical model for the site, one alternative would be to represent the section above the bedrock as three layers, each with a constant shear velocity given by the measured interval velocity. We rejected this alternative because, for one thing, it would have no increase in velocity with depth between 40 and 184 meters, which is unrealistic in view of the laboratory data previously cited, and, for another, it would introduce an artificial interface at 40 m. Guided by the results of Hardin and Black (1969) and Hardin and Drnevich (1972a, 1972b), we postulated that shear velocity is proportional to the one-fourth power of vertical effective stress both in the interval above 8 meters and in the interval from 8 meters to bedrock, but that the proportionality constants are different in the two intervals. A velocity-depth curve based on those assumptions was fitted to the measured travel-time data and is shown in Figure 6. In order to represent a smooth variation of velocity with depth, the section was divided into 67 constant-velocity layers with thicknesses of 0.5 meter near the surface ranging up to 5 meters at depth.

There were no measurements of shear velocity for the Franciscan bedrock. Seismic refraction profiles in the area (Hazlewood and Joyner, 1973; Hazlewood, 1974) give 3700 meters/sec for the P-wave velocity. An estimate of 2200 meters/sec was obtained for the shear velocity by assuming a V_s/V_p ratio of 0.6. Estimating the shear velocity from the P-wave velocity in soils can lead to seriously erroneous results, but for the bedrock it is a reasonable procedure. Furthermore, as long as the shear velocity contrast at the bedrock interface is large, the response is not highly sensitive to the bedrock velocity.

A value of Q for the alluvium was obtained from an analysis of the attenuation of artificially generated shear waves. The amplitudes of the Fourier components of the artificially generated pulses were presumed to be proportional to

$$\frac{1}{R} \exp\left(-\frac{\pi f R}{Q v_s}\right)$$

where R is the distance from the source and f is frequency. Two measurements of amplitude A_1 and A_2 at distances R_1 and R_2 can then be used to determine Q by the equation

$$Q = \frac{\pi f (R_2 - R_1)}{v_s \ln(A_1 R_1 / A_2 R_2)} . \qquad (1)$$

This equation is based on the low-loss approximation, but computations using the exact expression (Borcherdt, 1973, equation [72]) give values that differ by only one-tenth of one percent.

A similar approach was used by Kudo and Shima (1970) in measuring the Q of soils at sites in Japan. In using equation (5)', the value taken for v_s was the average shear velocity over the interval between the two measurements. Amplitudes measured at the instrument below the bedrock surface were corrected for the effect of transmission across the bedrock-soil interface using the following expression for the transmission coefficient at normal incidence (Medvedev, 1962, p. 52).

$$\frac{A'}{A} = \frac{2\rho v_s}{\rho v_s + \rho' v_s'} \qquad (6)$$

where ρ, v_s, and A denote, respectively, the density, shear velocity, and amplitude for the incident medium, and the primed quantities refer to the refracted medium. The value used for v_s was the interval velocity between the 40 m and 186 m levels. Using the values previously given for the other parameters, the transmission coefficient is 0.24.

Fourier amplitudes were calculated for 0.1 second lengths of the shear wave pulses recorded by Warrick (1974). The data were digitized at 320 samples per second and windowed as described in a previous section. The spectral amplitudes were not smoothed. The resulting values of Q are given in Table 2a for the different depth intervals and the frequencies within the band of dominant frequencies. Table 2b gives the Q values obtained from equation (5)' by using maximum trace amplitudes (corrected for transmission at the bedrock interface in the case of the record from 186 m) instead of Fourier amplitudes for A_1 and A_2 and by using for f the average of the estimated dominant frequencies of pulses at the two levels.

The interval from 12 to 40 meters is too short to give a reliable determination. For the other intervals, most of the Q values lie within a factor of 2 of the value 16, which was, somewhat arbitrarily, adopted for all the material from the surface to bedrock.

The data on the attenuation of artificial shear waves gave no information on the Q for material above the level of the instrument at 12 meters including in particular the material above 8 meters which has very different physical properties from the rest of the section. The applicability of a Q of 16 for the material above 8 meters was tested by comparing observed spectral ratios between the surface and 12 meters for a local earthquake (magnitude 3.6, distance 66 km) with predicted spectral ratios computed assuming different values of Q for the material above 8 meters (Figure 7). The predicted ratios shown on Figure 7 are based on the shear velocity distribution shown in Figure 6. A Q of 16 was assumed for the material below 8 meters, and predicted ratios were computed with Q values of 8, 16, and 32 for the material above 8 meters. Vertical incidence was assumed for the input wave in the bedrock, and the other parameters are as previously assigned. As will be shown subsequently, the assumed angle of incidence has essentially no effect on the results.

In comparing observed and predicted spectral ratios, it is necessary to take into account the effect of the data processing procedures used on the observed data, as discussed by Bakun (1971). The height and breadth of peaks on the observed spectral ratios are affected by the windowing and smoothing procedures described in an earlier section. In order to make the predicted ratios comparable to the observed ratios, the predicted ratios in Figure 7 were computed in the following special way, which was used for all comparisons of observed and predicted ratios: To obtain the predicted spectral ratio between the surface and 12 meters, the complex transfer function was calculated in the frequency domain for the theoretical model by the method described in the preceding section. The complex Fourier spectrum was then obtained for the observed seismogram at the 12-meter level (padded with zeros to prevent "wrap-around" error). The spectrum of the observed motion at the 12-meter level was multiplied by the transfer function to give the spectrum of a predicted surface motion, and that spectrum was inverted to produce a predicted time history for the surface. The predicted surface time history was then windowed, transformed to the frequency domain, and smoothed following the same procedure as used for computing observed spectra. The resulting predicted surface spectrum was divided by the observed spectrum at 12 meters to give the predicted spectral ratios shown on Figure 7.

The results given in Figure 7 suggest that it is reasonable to assign a Q of 16 to the material above 8 meters as well as to that below. They also suggest that the response is not highly sensitive to Q.

In order to compute predicted spectral ratios for comparison with the observed ratios, it is necessary to specify the angle of incidence of the incoming shear wave postulated in the underlying medium. For many of the recorded events it would be difficult to specify an angle of incidence, and, indeed, at least some of the incoming seismic energy is not in the form of simple plane shear waves. Fortunately, the results are virtually unaffected by varying the angle of incidence for the model considered here, which has a large contrast in shear velocity between soil and bedrock. Figure 8 shows the computed spectral ratios between surface and bedrock for incidence angles of 0°, 30°, 60°, and 80°. The spectral ratios plotted are simply the moduli of the theoretical transfer functions with no modifications to simulate windowing or smoothing. In view of the negligible effect of variations in incidence angle, all other predicted spectral ratios were computed for zero angle. The reader is cautioned that the comparisons of Figure 8 apply to ratios between surface of a soil layer and the bedrock directly beneath. They would not necessarily apply to ratios between a site with soil at the surface and a different site with bedrock at the surface. The similarity of the spectral ratios for different angles of incidence is not surprising if one notes that, while the angle of incidence in the bedrock varies from zero to 80°, the angle of refraction in the sediments varies only between zero and about 10° for the assumed velocities.

COMPARISON BETWEEN OBSERVATIONS AND MODEL PREDICTIONS

In order to emphasize the site characteristics and eliminate insofar as possible the effects of source and instrument response, we look at ratios of spectra between different levels. Of greatest interest is the ratio between the surface and the bedrock interface. On Figure 9 the predicted ratio is compared with the observed ratio for the north component from different segments of the recording of the San Fernando earthquake of 1971 (magnitude 6.6, distance 485 km). The predicted ratio was computed by the method described in the preceding section to simulate the effects of windowing and smoothing. The observed ratios are plotted only at those frequencies for which the signal-to-noise is at least two for both surface and bedrock spectra. The top curve on Figure 9 is the observed ratio for the 164 seconds of record shown in Figure 4. The next three curves are for non-overlapping 41-second segments, respectively, (1) at the beginning of the record (0-41 sec), (2) immediately following the estimated S arrival time (53-94 sec), and (3) near the end of the record (95-136 sec).

The first three response peaks in the predicted ratios can readily be identified in the observed ratios, and they occur at very nearly the predicted frequencies. The height of the observed and predicted peaks is comparable except for the last recorded segment, which gives peaks about twice the predicted values. It is doubtful that the bedrock motion for any of the three record segments represents only shear waves as postulated in the theoretical model. Nevertheless, the model gives a reasonable representation of the observed response.

The San Fernando earthquake was the only recorded event with adequate signal-to-noise ratio in the vicinity of 0.5 Hz to define the lowest frequency response peak. Observed spectral ratios between surface and bedrock (north component) are given in Figures 10 and 11 for all other recorded events with favorable signal-to-noise ratios in the range from about 1 to 5 Hz. The bottom curve in both figures is the predicted ratio copied from Figure 9. In all cases the second and third response peaks are present at approximately the predicted frequencies, and in most cases the height of observed and predicted peaks is comparable.

The similarity of the observed spectral ratios on Figures 9, 10, and 11 indicates that the spectral amplification at the site is relatively insensitive to the characteristics of the source. The earthquakes included represent a range in magnitude of 3.6-6.6, a range in epicentral distance of 29-485 km, and a variety of azimuths.

Gibbs and Borcherdt (1974) obtained an amplification spectrum for the site of the downhole array from surface recordings of a distant nuclear explosion. They took the spectral ratio between the recording at the downhole site and the recording at a nearby site on bedrock. Theoretically, the spectral ratio between recordings obtained at the surface of a soil layer and at the bedrock interface directly beneath is not the same as that between recordings at the surface of the soil layer and at a different site with bedrock at the surface. For large velocity contrasts between soil and bedrock, however, the two kinds of spectral ratios should show similar features. Figure 12 shows the spectral ratio (solid line) between the east component from the downhole site and the east component from a bedrock site at Black Mountain (Gibbs and Borcherdt, 1974). The theoretical ratio between soil surface and bedrock surface, computed from the model described in this report, is shown (dashed line) for comparison. The theoretical ratio is simply the modulus of the transfer function with no modifications to simulate windowing or smoothing. There is reasonably good agreement between the two curves. The first two peaks in the observed ratio of Figure 12 can readily be correlated with the corresponding peaks in the observed spectral ratios from the downhole array (Figures 9, 10, and 11).

Spectral ratios were also computed between the surface and 12 meters to show the response of the shallow, low-velocity material. Figure 13 gives the observed ratios for a representative sample of events along with the predicted ratio copied from Figure 7. The first two response peaks are clearly present in all cases at approximately the predicted frequency.

Comparisons were also made between observed and predicted surface time histories for two selected events (Figures 14, 15, and 16). For the San Fernando earthquake, the bottom trace in Figure 14 is the observed north component at the bedrock level, the middle trace is the observed north component at the surface, and the top trace is the north component at the surface predicted from the bedrock trace by the theoretical model. The predicted surface trace was obtained with the aid of the Fast Fourier Transform in the following manner. The bedrock trace was extended in time with zeros to prevent "wrap around" error. The complex transform of the extended trace was multiplied by the complex transfer function computed from the theoretical model. The product was then transformed back into the time domain to give the predicted surface trace.

In general, the theoretical model predicts the variation in time of amplitude and frequency content rather well. There is a low-frequency wave train apparent on the observed trace between about 120 and 140 seconds that is not well represented on the predicted trace. This probably represents a mode of propagation not allowed for in the simplified theoretical model. Figure 15 shows the central portion of the same traces at an expanded time scale. From Figure 15 it is clear that, although the amplitude level and the variations in frequency content with time are reasonably well predicted by the theoretical model, no correlation can be made of specific peaks or troughs between the observed and theoretical traces.

Figure 16 shows the same comparison for a local earthquake (magnitude 3.1, distance 79 km). As before, the bottom trace is the observed bedrock motion, the middle trace the observed surface motion, and the top trace the surface motion predicted by the theoretical model. The excitation in this case is much higher frequency than for the previous example, but the conclusion is similar. The theoretical model predicts the variations in amplitude level with time reasonably well. The comparison is better for the high amplitude shear wave train starting at about 16 seconds than it is for the earlier portion of the record.

DISCUSSION

The effects of the soil on low-amplitude ground motion were observed for a variety of earthquake sources at a site where the lateral extent of the soil layers is large compared to the total thickness and where the shear velocity contrast between soil and bedrock is large. The observed effects at this site are reasonably well accounted for by a simple, plane-layered model with material properties determined independently. For the horizontal spectral ratios between the surface and bedrock, the model predicts the frequencies of the first three peaks within 10 percent in most cases and the height of the peaks within about 50 percent in most cases.

Surface time histories computed from the theoretical model predict the time variations of amplitude and frequency content reasonably well, but correlation of individual cycles cannot be made between observed and predicted traces. Given the long complex wave trains characteristic of our data, the lack of detailed correlation is not particularly surprising in view of our incomplete knowledge of the distribution of material properties with depth and the oversimplifications that are undoubtedly involved in the plane-layered model.

These results agree in general with those reported for other downhole arrays. Shima (1962) analyzed data from arrays at Tokyo Station and Seed and Idriss (1970) analyzed data from an array at Union Bay, Seattle. In both cases, general agreement was reported between the observations and the predictions of simple plane-layer theory. Tsai and Housner (1970) in their analysis of the Union Bay data adjusted the parameters of their model to obtain the best fit between observations and theoretical predictions. Very good agreement was obtained. The value of damping determined for the first mode, however, was 10 percent of critical, a value that they considered much higher than could reasonably be ascribed to internal energy dissipation. They attributed the high value to the effect of departures from the simple assumptions of plane waves traveling through plane layers. Dobry, Whitman, and Roesset (1971) came to a similar conclusion from analysis of both the Union Bay and Tokyo Station data.

For the one event in which we observed the first mode peak, the data from our site do not require such high damping values. Our estimate of Q for the soil, obtained from independent measurements, was 16, which corresponds to a damping value of about three percent of critical. The theoretical spectral ratios calculated on that basis agreed reasonably well with the observed ratios for the San Fernando earthquake (Figure 9).

The high damping values obtained by Tsai and Housner (1970) and Dobry, Whitman, and Roesset (1971) at the Union Bay and Tokyo Station sites may indeed represent losses of energy associated with departures from the simple assumptions of the plane-layer model. If so, however, the relative importance of such losses should diminish as one proceeds to the prediction of response at high levels of motion where the energy loss in nonlinear deformation is large.

In summary, our results provide further evidence that, under favorable conditions, simple plane-layer models are capable of giving reasonably good approximations of the effects of local soil conditions on low-amplitude ground motion. Extension to the prediction of effects at high amplitude levels requires measures to take account of the nonlinear behavior of soil at high strain. Methods to accomplish this extension have been described by a number of authors (e.g., Joyner and Chen, 1975; Streeter, Wylie, and Richart, 1974; Hardin and Drnevich, 1972b; Idriss and Seed, 1968b). Adequate empirical verification of these methods awaits the collection and analysis of additional strong motion data.

ACKNOWLEDGMENTS

We are indebted to Jerry P. Eaton for advice and encouragement during the initial stages of the investigation, to Roger D. Borcherdt for advice on theoretical problems in linear viscoelasticity, to Harold W. Olsen for unpublished data on soil properties at the site and for his advice on questions of soil dynamics, and to Samuel W. Stewart for suggesting the use of the Haskell matrix method. William H. Bakun and Roger D. Borcherdt read the manuscript and made valuable suggestions. We are grateful to Edward F. Roth for his assistance in the operation and maintenance of the recording system. The San Francisco Water Department gave permission to operate the recording array on their property. The research for this paper was done in cooperation with the Division of Reactor Research and Development, U.S. Atomic Energy Commission.

REFERENCES

Adams, R. D., and B. S. Gopalakrishnan (1971). Earthquakes and the registration of earthquakes from July 1, 1970, to December 31, 1970, Bull. Seism. Stations, University of California, Berkeley, 40, 119-234.

Allen, C. R., G. R. Engen, T. C. Hanks, J. M. Nordquist, and W. R. Thatcher (1971). Main shock and larger aftershocks of the San Fernando earthquake, February 9 through March 1, 1971, in The San Fernando, California, Earthquake of February 9, 1971, U.S. Geol. Surv. Profess. Paper 733, 17-20.

Bakun, W. H. (1971). Crustal model parameters from P-wave spectra, Bull. Seism. Soc. Am., 61, 913-935.

Borcherdt, R. D. (1970). Effects of local geology on ground motion near San Francisco Bay, Bull. Seism. Soc. Am., 60, 29-61.

Borcherdt, R. D. (1973). Energy and plane waves in linear viscoelastic media, J. Geophys. Res., 78, 2442-2453.

Borcherdt, R. D., E. E. Brabb, W. B. Joyner, E. J. Helley, K. R. Lajoie, R. A. Page, R. L. Wesson, and T. L. Youd (1975). Predicted geologic effects of a postulated earthquake, in Studies for Seismic Zonation of the San Francisco Bay Region, U.S. Geol. Surv. Profess. Paper 941A, 88-95.

Campbell, K. W., and C. M. Duke (1974). Bedrock intensity attenuation and site factors from San Fernando earthquake records, Bull. Seism. Soc. Am., 64, 173-185.

Cloud, W. K., and A. Qamar (1972). Earthquakes and the registration of earthquakes from January 1, 1971, to June 30, 1971, Bull. Seism. Stations, University of California, Berkeley, 41, 1-102.

Cloud, W. K., J. Litehiser, and J. F. Tomblin (1972). Earthquakes and the registration of earthquakes from July 1, 1971, to December 31, 1971, Bull. Seism. Stations, University of California, Berkeley, 41, 103-225.

Cloud, W. K., W. Smith, and R. Uhrhammer (1974a). Earthquakes and the registration of earthquakes from July 1, 1972, to December 31, 1972, Bull. Seism. Stations, University of California, Berkeley, 42, 123-257.

Cloud, W. K., L. Hutchings, and E. Majer (1974b). Earthquakes and the registration of earthquakes from January 1, 1973, to June 30, 1973, Bull. Seism. Stations, University of California, Berkeley, 43, 1-111.

Dobry, R., R. V. Whitman, and J. M. Roesset (1971). Soil properties and the one-dimensional theory of earthquake amplification, Research Report R71-18, Department of Civil Engineering, Massachusetts Institute of Technology, 347 pp.

Espinosa, A. F., G. H. Sutton, and H. J. Miller (1962). A transient technique for seismograph calibration, Bull. Seism. Soc. Am., 52, 767-779.

Futterman, W. I. (1962). Dispersive body waves, J. Geophys. Res., 67, 5279-5291.

Gibbs, J. F., and R. D. Borcherdt (1974). Effects of local geology on ground motion in the San Francisco Bay region, California--a continued study, U.S. Geol. Surv. Open-File Report, 74-222, 146 pp.

Hardin, B. O., and W. L. Black (1969). Vibration modulus of normally consolidated clay (discussion), Proc. Am. Soc. Civil Eng., Journ. Soil Mech. and Found. Div., 95, 1531-1537.

Hardin, B. O., and V. P. Drnevich (1972a). Shear modulus and damping in soils: Measurement and parameter effects, Proc. Am. Soc. Civil Eng., Journ. Soil Mech. and Found. Div., 98, 603-624.

Hardin, B. O., and V. P. Drnevich (1972b). Shear modulus and damping in soils: Design equations and curves, Proc. Am. Soc. Civil Eng., Journ. Soil Mech. and Found. Div., 98, 667-692.

Haskell, N. A. (1953). The dispersion of surface waves on multilayered media, Bull. Seism. Soc. Am., 43, 17-34.

Haskell, N. A. (1960). Crustal reflection of plane SH waves, J. Geophys. Res., 65, 4147-4150.

Hazlewood, R. M. (1974). Preliminary report of seismic refraction survey along the east side of the San Francisco Bay, Alameda County, California, U.S. Geol. Surv. Open-File Report, 10 pp.

Hazlewood, R. M. and W.B. Joyner (1973). Prelininary report of seismic refraction survey, Redwood Shores, San Mateo County, California, U.S. Geol. Surv. Open-File Report, 9 pp.

Hudson, D. E. (1972). Strong motion seismology, Proceedings of the International Conference on Microzonation, Seattle, Washington, Vol. I, 29-60.

Idriss, I. M., and H. B. Seed (1968a). Seismic response of horizontal soil layers, Proc. Am. Soc. Civil Eng., Journ. Soil Mech. and Found. Div., 94, 1003-1031.

Idriss, I. M., and H. B. Seed (1968b). An analysis of ground motions during the 1957 San Francisco earthquake, Bull. Seism. Soc. Am., 58, 2013-2032.

Johnson, A. I., R. P. Moston, and D. A. Morris (1968). Physical and hydrologic properties of water-bearing deposits in subsiding areas in central California, U.S. Geol. Surv. Profess. Paper 497-A.

Joyner, W. B., and A.T.F. Chen (1975). Calculation of nonlinear ground response in earthquakes, Bull. Seism. Soc. Am. (in press).

Kanai, K. (1952). Relation between the nature of surface layer and the amplitudes of earthquake motions, Bull. Earthq. Res. Inst., Tokyo Univ., 30, 31-37.

Kanasewich, E. R. (1973). Time Sequence Analysis in Geophysics, University of Alberta Press, Edmonton, Alberta.

Kudo, K., and E. Shima (1970). Attenuation of shear waves in soil, Bull. Earthq. Res. Inst., Tokyo Univ., 48, 145-158.

Lajoie, K. R., and E. J. Helley (1975). Differentiation of sedimentary deposits for seismic zonation, in Studies for Seismic Zonation of the San Francisco Bay Region, U.S. Geol. Surv. Profess. Paper 941A, 39-51.

Lee, W.H.K., J. C. Roller, K. L. Meagher, and R. E. Bennett (1972a). Catalog of earthquakes along the San Andreas fault system in central California for the year 1970, U.S. Geol. Surv. Open-File Report.

Lee, W.H.K., K. L. Meagher, R. E. Bennett, and E. E. Matamoros (1972b). Catalog of earthquakes along the San Andreas fault system in central California for the year 1971, U.S. Geol. Surv. Open-File Report.

Matthiesen, R. B., C. M. Duke, D. J. Leeds, and J. C. Fraser (1964). Site characteristics of southern California strong motion earthquake stations, Part II, Report No. 64-15, Department of Engineering, University of California, Los Angeles.

Medvedev, S. V. (1962). Engineering Seismology, translation by the Israel Program for Scientific Translations, 1965, available from the Clearinghouse, Springfield, Virginia 22151.

Murphy, J. R., A. H. Davis, and N. L. Weaver (1971). Amplification of seismic body waves by low-velocity surface layers, Bull. Seism. Soc. Am., 61, 109-145.

Newmark, N. M., A. R. Robinson, A.H.-S. Ang, L. A. Lopez, and W. J. Hall (1972). Methods for determining site characteristics, Proceedings of the International Conference on Microzonation, Seattle, Washington, Vol. I, 113-129.

Schlocker, J. (1970). Generalized geologic map of the San Francisco Bay region, California, U.S. Geol. Surv. Open-File Map.

Schnabel, P., H. B. Seed, and J. Lysmer (1972). Modification of seismograph records for effects of local soil conditions, Bull. Seism. Soc. Am., 62, 1649-1664.

Seed, H. B., and I. M. Idriss (1970). Analysis of ground motions at Union Bay, Seattle, during earthquakes and distant nuclear blasts, Bull. Seism. Soc. Am., 60, 125-136.

Seed, H. B., and P. Schnabel (1972). Soil and geologic effects on site response during earthquakes, Proceedings of the International Conference on Microzonation, Seattle, Washington, Vol. I, 61-85.

Shima, E. (1962). Modifications of seismic waves in superficial soil layers as verified by comparative observations on and beneath the surface, Bull. Earthq. Res. Inst., Tokyo Univ., 40, 187-259.

Streeter, V. L., E. B. Wylie, and F. E. Richart (1974). Soil motion computations by characteristics method, Proc. Am. Soc. Civil Eng., Journ. Geotechnical Eng. Div., 100, 247-263.

Treasher, R. C. (1963). Geology of the sedimentary deposits in San Francisco Bay, California, in Short Contributions to California Geology, Special Report 82, California Division of Mines and Geology, 11-24.

Tsai, N. C., and G. W. Housner (1970). Calculation of surface motions of a layered half-space, Bull. Seism. Soc. Am., 60, 1625-1651.

Warrick, R. E. (1974). Seismic investigation of a San Francisco Bay mud site, Bull. Seism. Soc. Am., 64, 375-385.

Wesson, R. L., K. L. Meagher, and F. W. Lester (1973). Catalog of earthquakes along the San Andreas fault system in central California, July-September 1972, U.S. Geol. Surv. Open-File Report.

Wesson, R. L., F. W. Lester, and K. L. Meagher (1974a). Catalog of earthquakes along the San Andreas fault system in central California, October-December 1972, U.S. Geol. Surv. Open-File Report.

Wesson, R. L., F. W. Lester, and K. L. Meagher (1974b). Catalog of earthquakes along the San Andreas fault system in central California, January-March 1973, U.S. Geol. Surv. Open-File Report.

Wood, H. O. (1908). Distribution of apparent intensity in San Francisco, in The California Earthquake of April 18, 1906, Report of the State Earthquake Investigation Commission, Carnegie Inst. of Wash., Publ. 87, Washington, D.C., 220-245.

APPENDIX

SYSTEM RESPONSE TESTS

The use of spectral ratios between motion recorded at different levels is intended to remove the effects of source and instrument characteristics and exhibit the effect of site characteristics alone. This depends upon similarity in instrument response. To check the relative response of the instruments *in situ*, we subjected them to the following test: A known voltage was applied to the terminals of the cable leading to the downhole seismometer. The resulting current in the seismometer coil caused the mass to be displaced. The voltage was maintained for a time sufficient to allow the system to reach equilibrium at the displaced position. Then, using a fast-acting, bounce-free switching system, the voltage was removed, and the terminals were connected to the amplifier input, giving a recording of the transient signal produced as the seismometer mass returned to its original equilibrium position. To avoid spurious transients in the amplifier system, a shunt resistance equal to that represented by the seismometer and cable was connected to the input terminals of the amplifier during the time when the seismometer cable was disconnected. Test results are shown in Figure 17 for the six horizontal instruments from the three levels most used in the subsequent interpretation, surface, 12 meters, and 186 meters.

Shima (1962) used the same technique for *in situ* calibration of downhole seismometers. The technique is not new. A discussion with references to earlier work is given by Espinosa, Sutton, and Miller (1962).

The input represented by the test is the equivalent of a step in acceleration. We obtain an expression for the amplitude of the step in terms of the electrodynamic constant G given by

$$G = F/I$$

where F is the force on the seismometer mass produced by a current I in the coil. Since

$$I = E/R$$

where E is the applied voltage and R is the resistance of the cable and seismometer, the equivalent acceleration step has an amplitude of

$$-\frac{GE}{mR}$$

where m is the seismometer mass.

We can compare the response of different channels of the system by taking ratios of the output spectra from the tests. Since the equivalent input depends upon (G/(mR), which might conceivably vary from one seismometer to the next, this comparison does not test the relative overall gain level between channels. It does, however, test whether or not the shapes of the spectral response curves are similar, since the shapes of the input spectra are the same. Results are shown in Figure 18 which gives the spectral ratios comparing five of the horizontal seismometer channels to a reference channel, which was the north-south surface instrument. Before computing the spectra used for the ratios plotted in Figure 18, the time-domain data were multiplied by the 10-percent window described in the text in order to minimize leakage. The spectra were <u>not</u> smoothed.

All the ratios shown in Figure 18 are reasonably flat except for the one at the bottom which represents the east-west surface instrument and which shows anomalously high response below 0.5 Hz. The problem with the east-west surface instrument disappeared spontaneously on a later test, but the test illustrated in Figure 18 must be presumed representative of the period of time in which the most significant records were obtained. For that reason we limited all analysis to the north component.

The calibration test data can be used to determine the response of the whole system (seismometer, amplifier, recorder, and digitizer) as a function of frequency. The test input is the equivalent of a step in acceleration with amplitude

$$A = \frac{GE}{mR} .$$

This corresponds to a ramp in velocity with slope A. The spectrum of the equivalent velocity input is $A/(2\pi f)^2$, where f is frequency. The response of the channel to a velocity inpulse can therefore be obtained by dividing the spectrum of the test output by $A/(2\pi f)^2$. This was done for the surface north-south channel using a value for G from damping tests made prior to installation and a value for m given by the manufacturer. The results are shown by the x's in Figure 19, which can be compared to the theoretical response for the geophone alone (solid line in Figure 19). The decrease in the total system response relative to the theoretical seismometer response below about 0.5 Hz represents primarily the effect of the transformer coupling at the amplifier input. The difference in overall level probably represents the error in determining the electrodynamic constant.

TABLE 1

List of Earthquakes

Event	Date	Origin time (GMT)	Latitute North	Longitude West	Depth (km)	Magnitude	Distance (km)	Azimuth (deg)
Pittsburg	70 08 31	12 12 58.9	38°04.7'	121°57.4'	6.0	3.6	66	13
Anzar	70 09 18	09 34 12.6	36°55.1'	121°35.9'	6.5	3.1	79	143
San Fernando	71 02 09	14 00 41.6	34°24.0'	118°23.7'	13.0	6.6	485	135
Laurel	71 02 22	20 39 12.6	37°06.3'	121°58.5'	14.0	2.8	45	164
Gordo Escarpment	71 02 27	00 31 37.7	40°16'	124°50'	5.2	5.2	384	323
Gilroy	71 06 19	08 17 58.5	36°58.1'	121°39.0'	5.5	3.7	72	144
Castro Valley	71 12 11	21 35 12.2	37°45.2'	122°08.1'	5.8	3.4	29	358
Bear Valley 1	72 09 04	18 04 40.8	36°37.5'	121°16.5'	5.7	4.7	123	142
Salinas 1	72 10 03	06 30 02.3	36°48.1'	121°31.7'	5.0	4.8	93	146
Salinas 2	72 10 03	11 10 13.6	36°48.8'	121°32.7'	5.1	4.1	92	146
Bear Valley 2	73 01 15	09 43 29.9	36°40.3'	121°20.0'	6.3	4.1	116	142

TABLE 2

Q Values

a. Using Fourier Spectral Amplitudes

Frequency	Interval		
	12-40 m	12-186 m	40-186 m
10	-213	7.3	5.6
20	88	14.6	11.7
30	52	20.8	17.6
40	-19	28.4	16.4
50	651	22.4	17.4

b. Using Maximum Trace Amplitudes

Interval		
12-40 m	12-186 m	40-186 m
9.1	15.1	18.5

LIST OF ILLUSTRATIONS

Figure 8. Horizontal spectral ratios between the surface and 186 meters, computed for the model described in the text with different angles of incidence, ϕ. The ratios were computed without modifications to simulate windowing or smoothing.

Figure 9. Horizontal spectral ratios between the surface and 186 meters. Computed ratio for the model is compared with observed ratios for the north component from different segments of the record of the San Fernando earthquake, as described in the text.

Figure 10. Horizontal spectral ratios between the surface and 186 meters. Computed ratio for the model is compared with observed ratios for the north component from the earthquakes indicated (Table 1). For each earthquake 41 seconds of data following the P arrival were used.

Figure 11. Horizontal spectral ratios between the surface and 186 meters. Computed ratio for the model is compared with observed ratios for the north component from the earthquakes indicated (Table 1). For the Gordo Escarpment earthquake, 41 seconds of data following the S arrival were used; for Bear Valley 1, 82 seconds of data following the P arrival were used; and for the other two, 41 seconds following the P arrival.

Figure 12. Horizontal spectral ratios between the downhole site and a site with bedrock at the surface. The solid curve is the observed ratio for a distant nuclear explosion (Gibbs and Borcherdt, 1974). The dashed curve is the corresponding theoretical ratio calculated for the model described in this report.

Figure 13. Horizontal spectral ratios between the surface and 12 meters. Computed ratio for the model is compared with observed ratios for the north component from the earthquakes indicated. For each earthquake 41 seconds of data following the P arrival were used.

Figure 14. Comparison of computed and observed motion for the north component from the San Fernando earthquake.

Figure 15. Comparison of computed and observed motion for the north component from a portion of the San Fernando earthquake record.

Figure 16. Comparison of computed and observed motion for the north component from the Anzar earthquake (magnitude 3.1, distance 79 km).

Figure 17. Instrument response tests for horizontal seismometers at the surface, 12 meters and 186 meters.

Figure 18. Spectral ratios from instrument response tests shown in Figure 17.

Figure 19. System response for the north seismometer channel at the surface, shown by the x's, compared with the theoretical geophone response given by the line. Units of response are microvolts per cm/sec.

Fig. 1

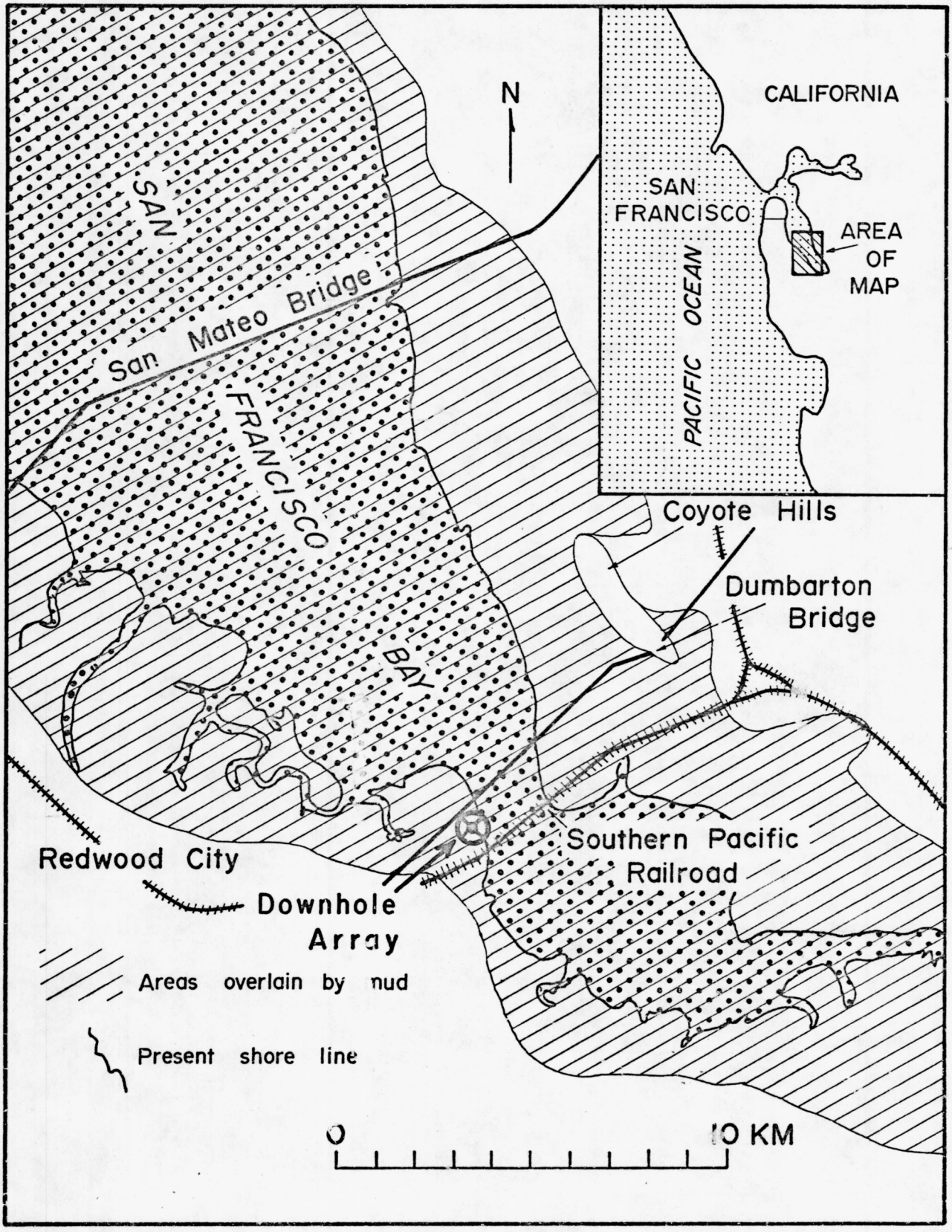
N
CALIFORNIA
SAN FRANCISCO
AREA OF MAP
PACIFIC OCEAN
SAN
San Mateo Bridge
FRANCISCO
BAY
Coyote Hills
Dumbarton Bridge
Redwood City
Southern Pacific Railroad
Downhole Array
Areas overlain by mud
Present shore line
0
10 KM

Fig. 2

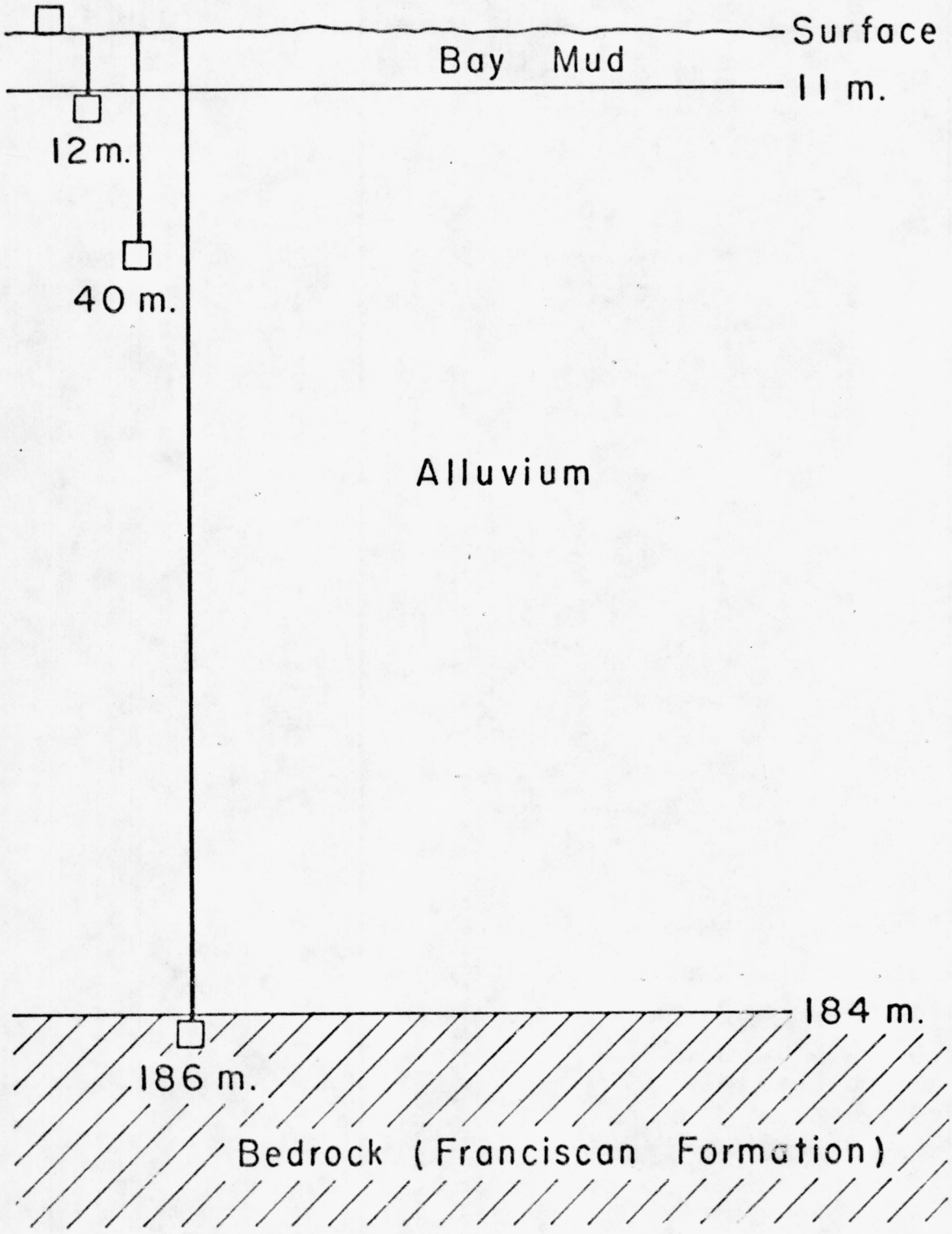
Surface
Bay Mud
11 m.
12 m.
40 m.
Alluvium
184 m.
186 m.
Bedrock (Franciscan Formation)

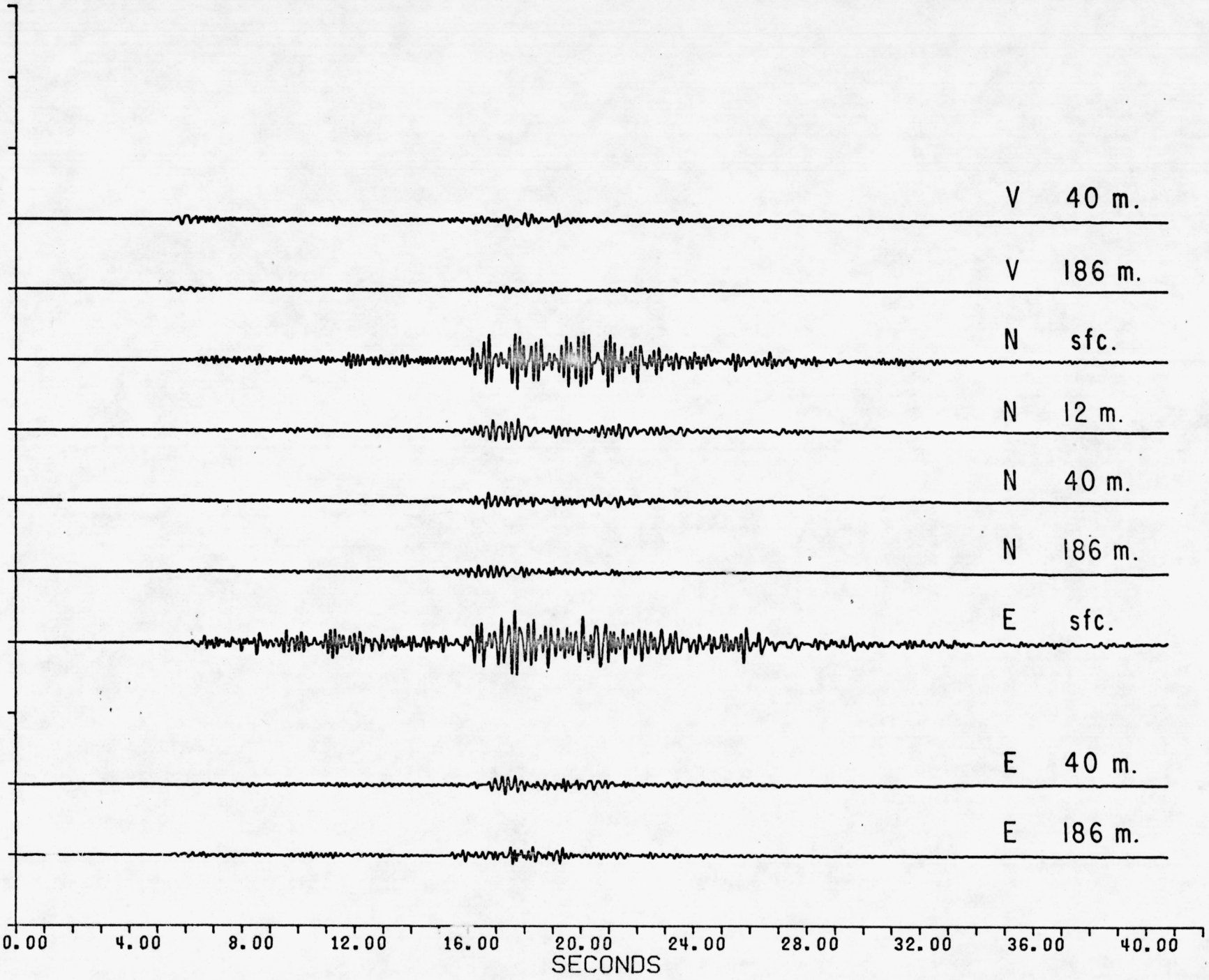
V 40 m.
V 186 m.
N sfc.
N 12 m.
N 40 m.
N 186 m.
E sfc.
E 40 m.
E 186 m.
0.00
4.00
8.00
12.00
16.00
20.00
24.00
28.00
32.00
36.00
40.00
SECONDS

Fig 3

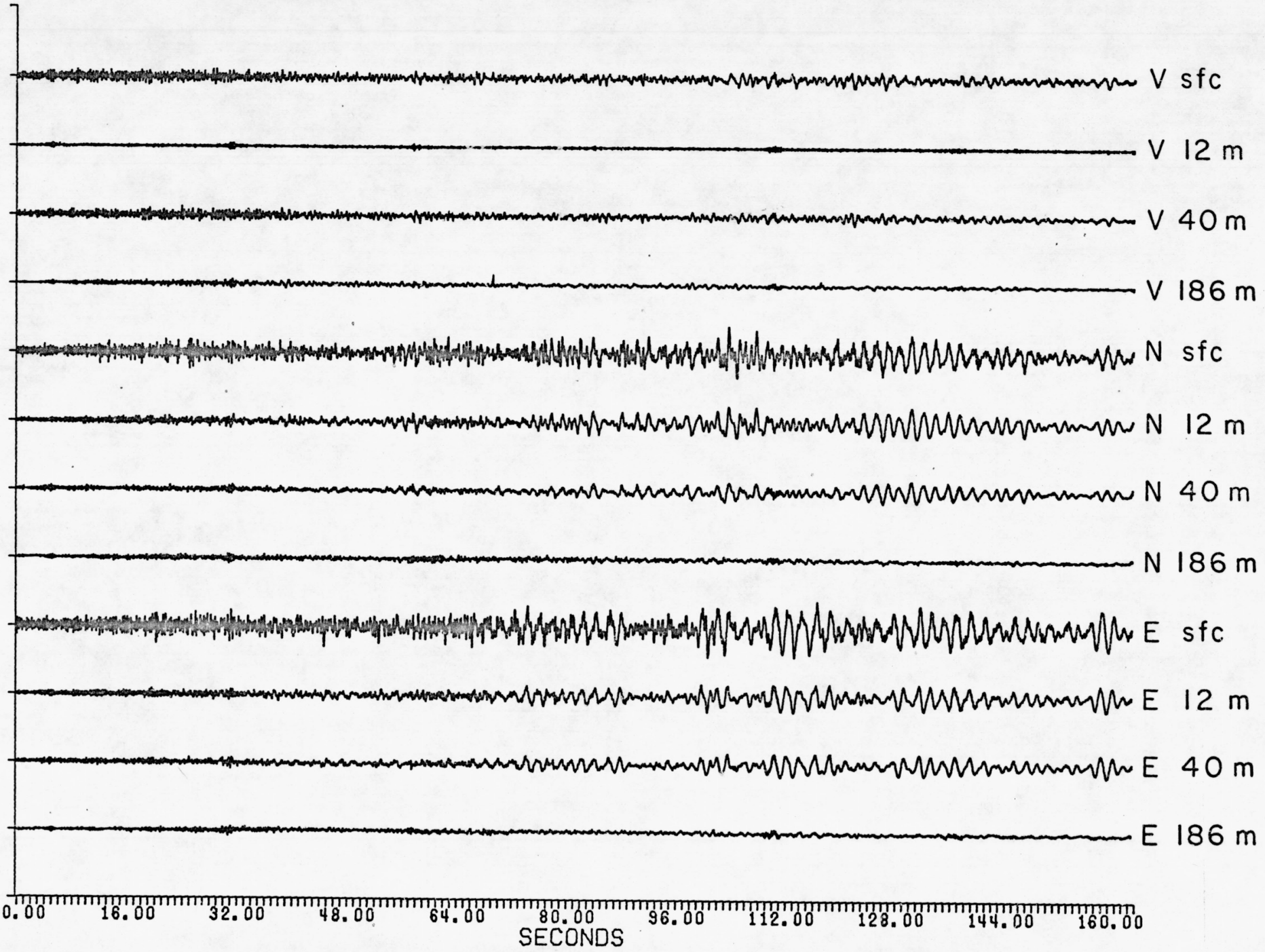
V sfc
V 12 m
V 40 m
V 186 m
N sfc
N 12 m
N 40 m
N 186 m
E sfc
E 12 m
E 40 m
E 186 m
0.00
16.00
32.00
48.00
64.00
80.00
96.00
112.00
128.00
144.00
160.00
SECONDS

Fig. 4

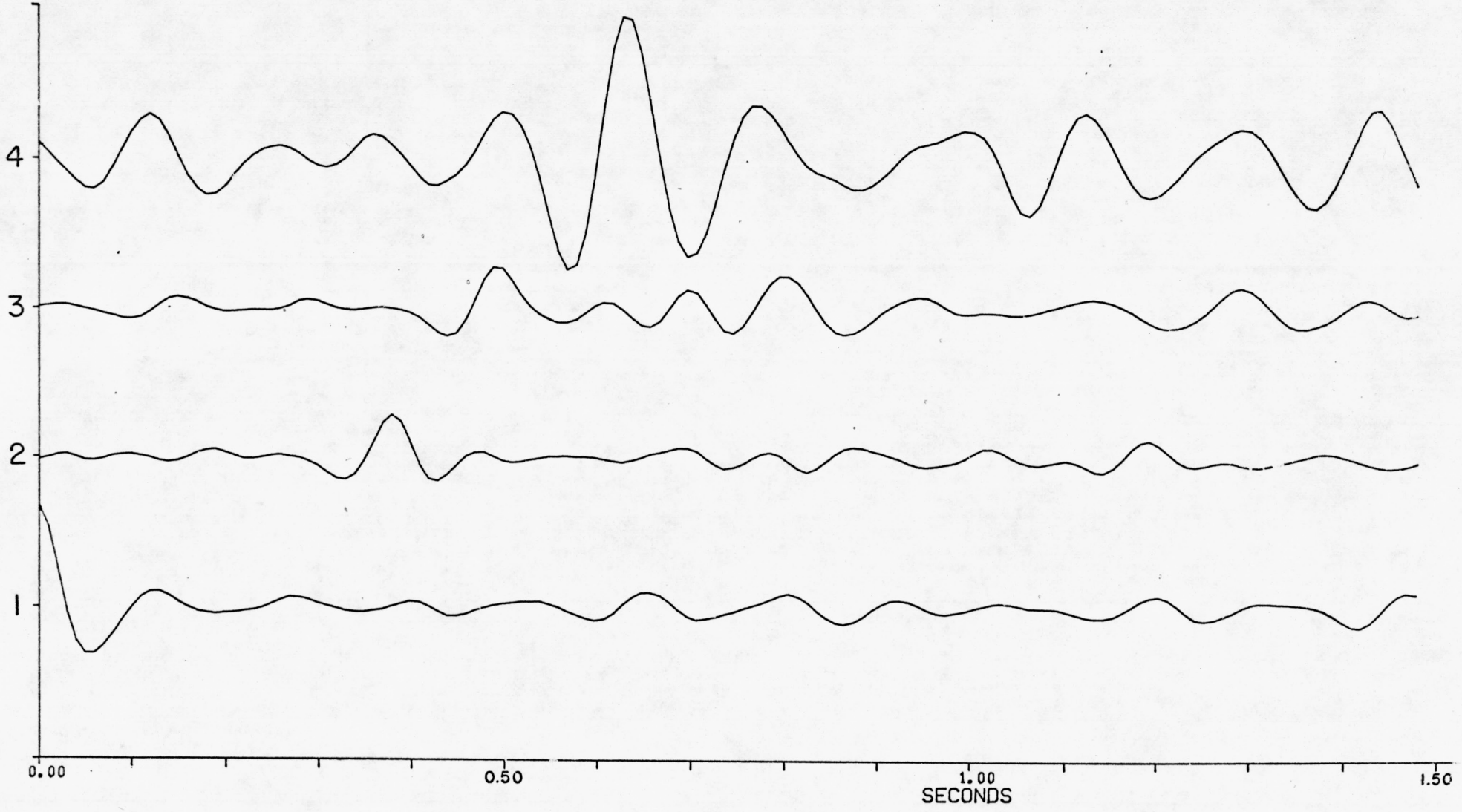

Fig. 5

Fig. 6

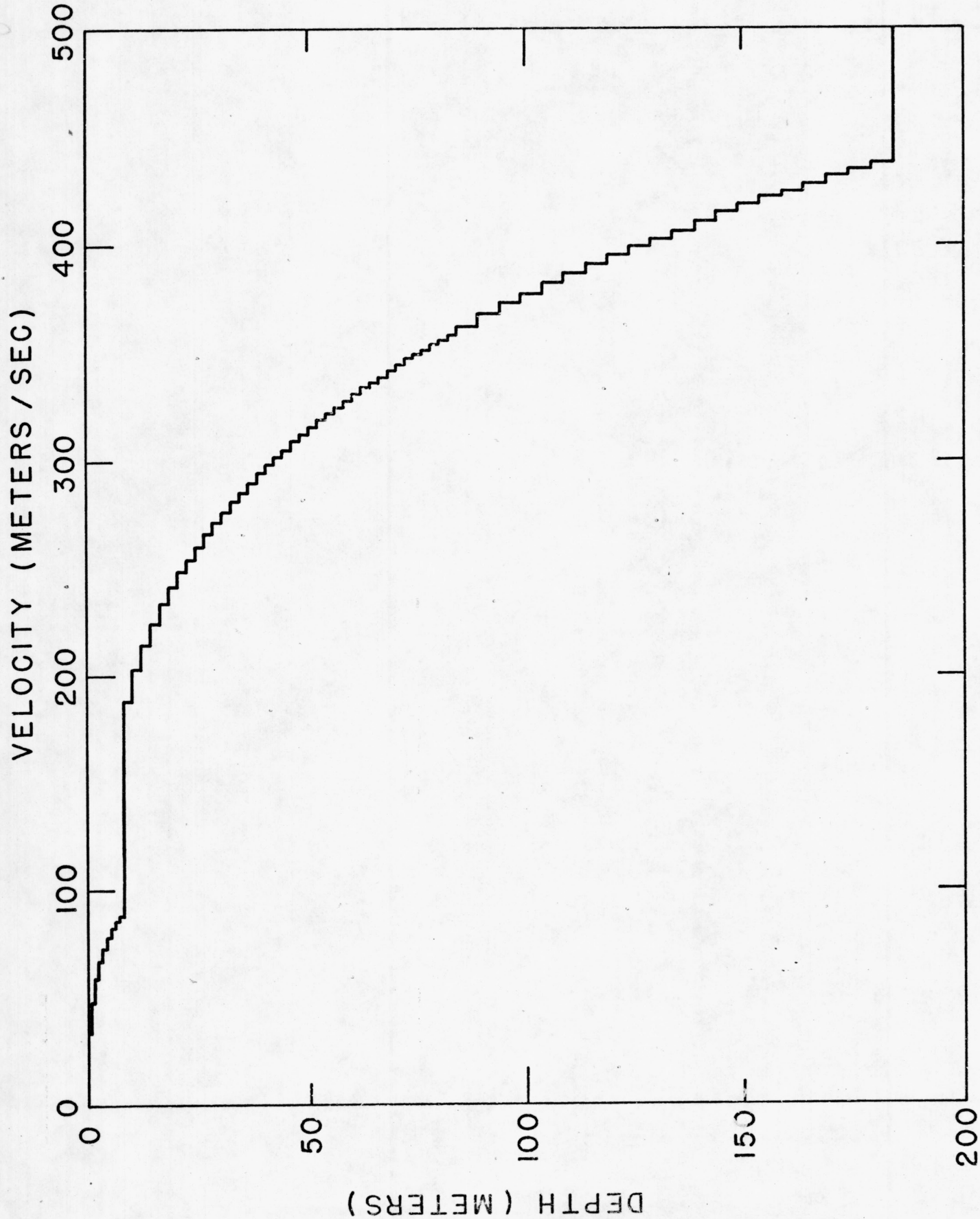
VELOCITY (METERS / SEC)
0
100
200
300
400
500
DEPTH (METERS)
0
50
100
150
200

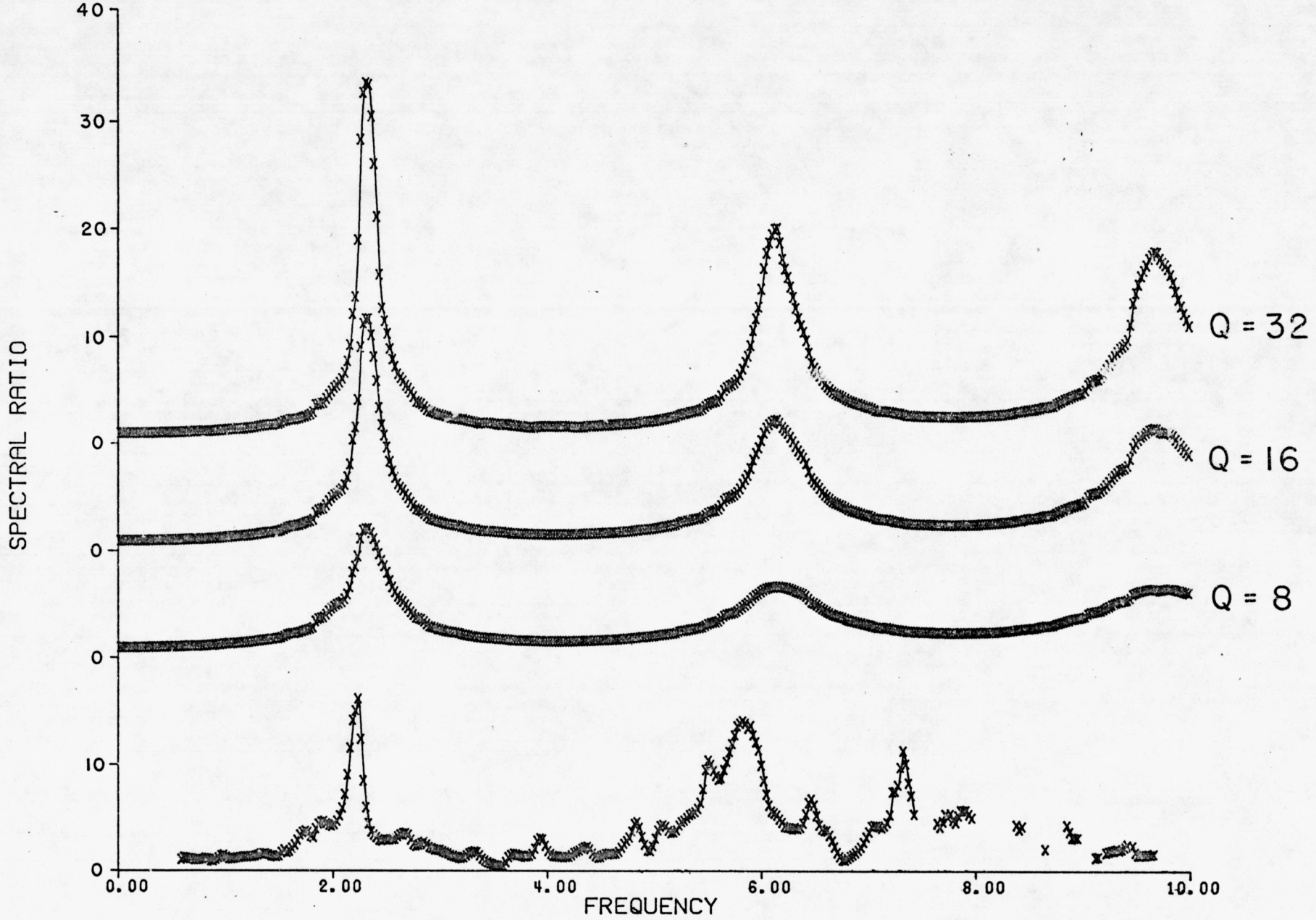
SPECTRAL RATIO
40
30
20
10
0
0
0
10
0
0.00
2.00
4.00
6.00
8.00
10.00
FREQUENCY
Q = 32
Q = 16
Q = 8

Fig. 7

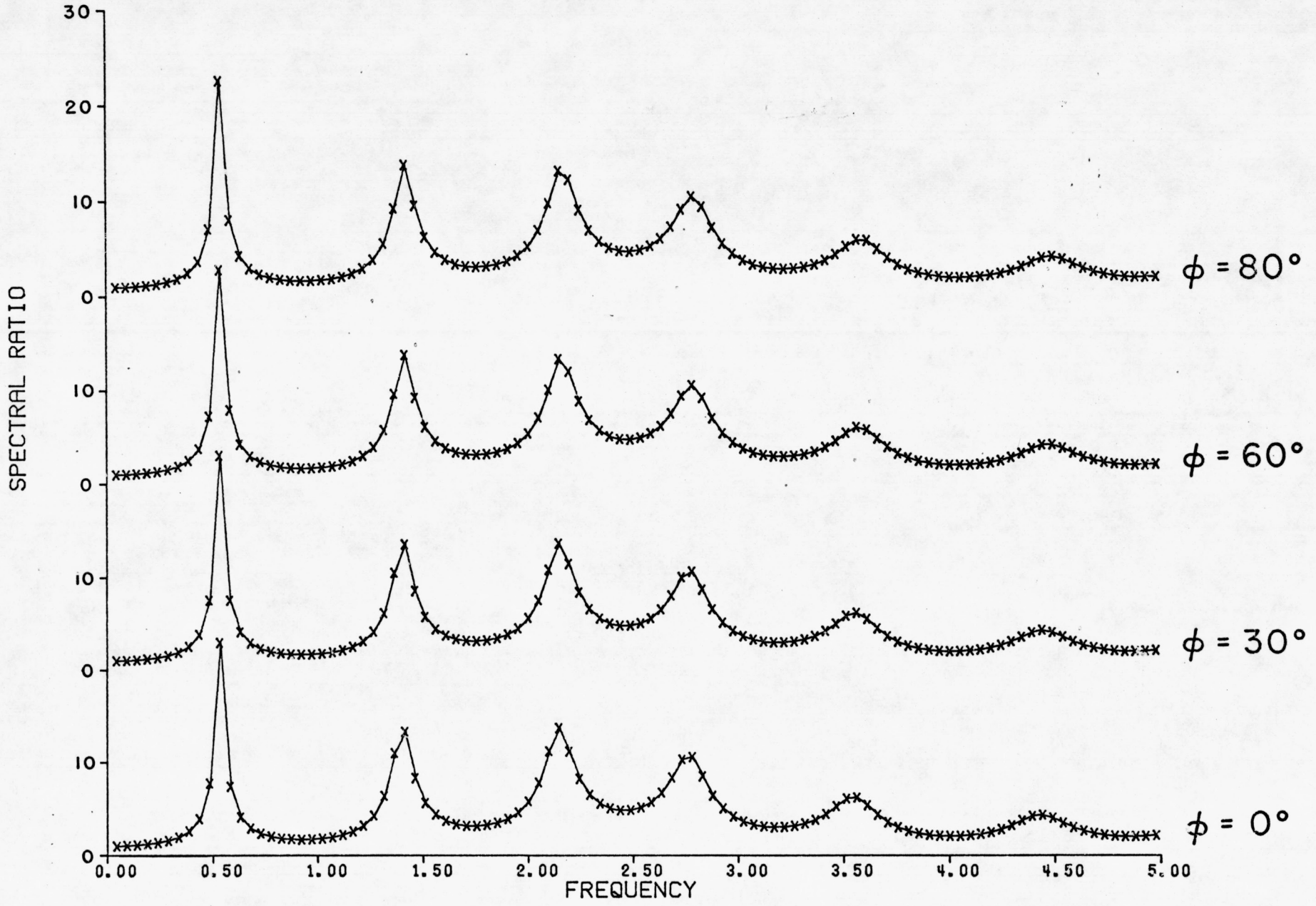
SPECTRAL RATIO
30
20
10
0
10
0
10
0
10
0
0.00
0.50
1.00
1.50
2.00
2.50
3.00
3.50
4.00
4.50
5.00
FREQUENCY
φ = 80°
φ = 60°
φ = 30°
φ = 0°

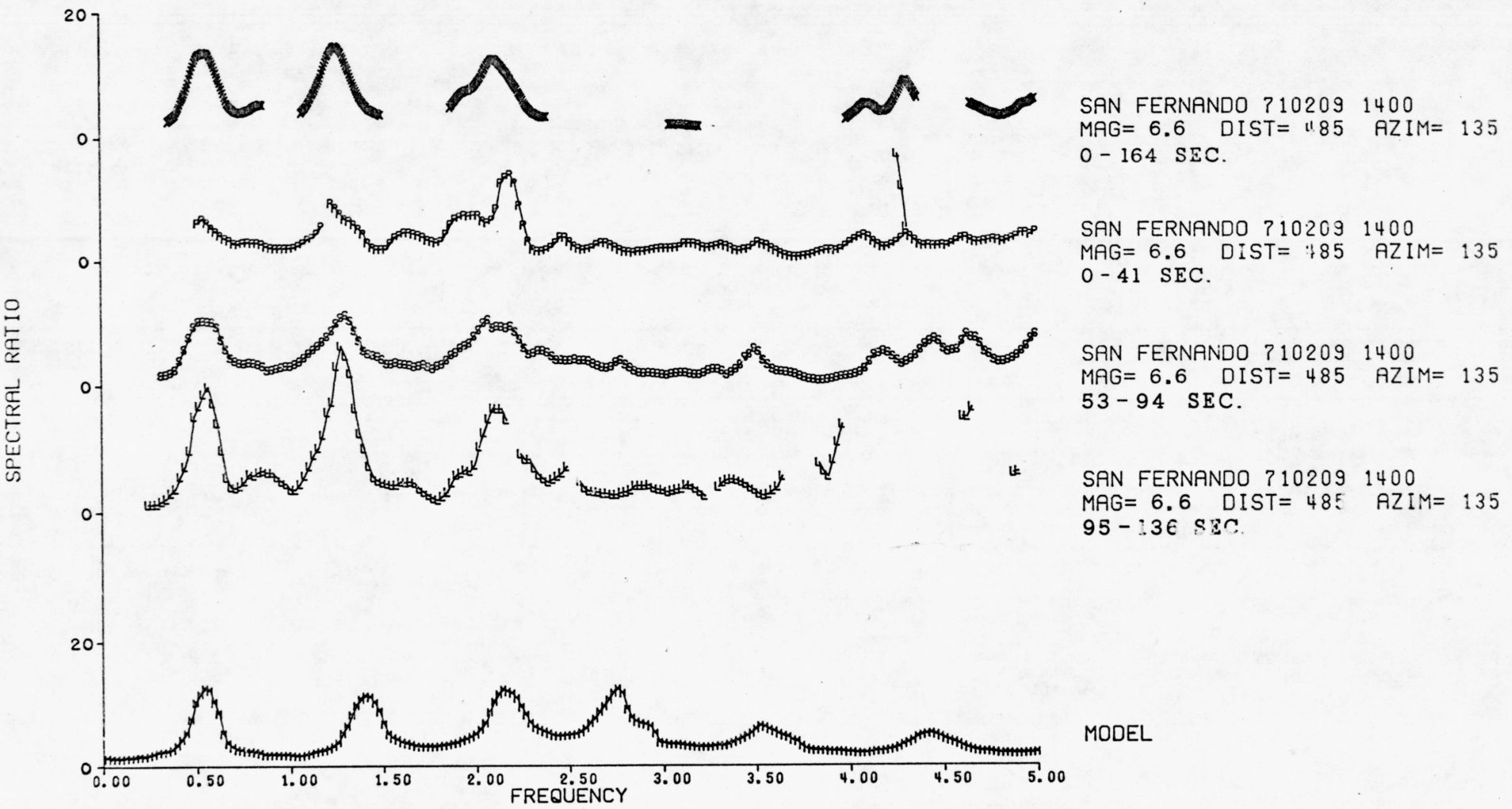
SPECTRAL RATIO
20
0
0
0
0
20
0
0.00
0.50
1.00
1.50
2.00
2.50
3.00
3.50
4.00
4.50
5.00
FREQUENCY
SAN FERNANDO 710209 1400
MAG= 6.6 DIST= 485 AZIM= 135
0 - 164 SEC.
SAN FERNANDO 710209 1400
MAG= 6.6 DIST= 485 AZIM= 135
0 - 41 SEC.
SAN FERNANDO 710209 1400
MAG= 6.6 DIST= 485 AZIM= 135
53 - 94 SEC.
SAN FERNANDO 710209 1400
MAG= 6.6 DIST= 485 AZIM= 135
95 - 136 SEC.
MODEL

Fig. 9

Fig. 9

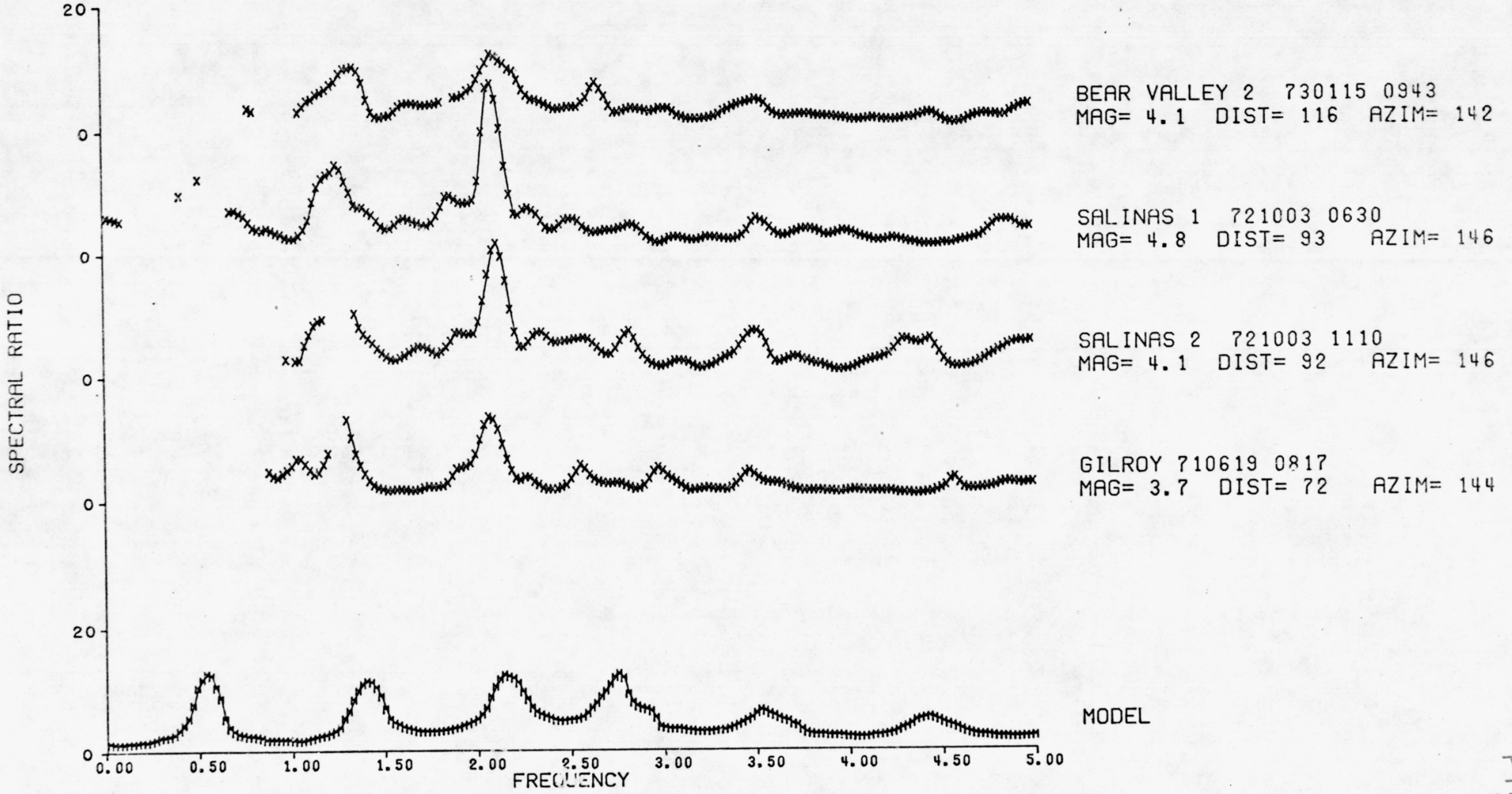
20
0
0
0
0
20
0
SPECTRAL RATIO
0.00
0.50
1.00
1.50
2.00
2.50
3.00
3.50
4.00
4.50
5.00
FREQUENCY
BEAR VALLEY 2 730115 0943
MAG= 4.1 DIST= 116 AZIM= 142
SALINAS 1 721003 0630
MAG= 4.8 DIST= 93 AZIM= 146
SALINAS 2 721003 1110
MAG= 4.1 DIST= 92 AZIM= 146
GILROY 710619 0817
MAG= 3.7 DIST= 72 AZIM= 144
MODEL

Fig. 10

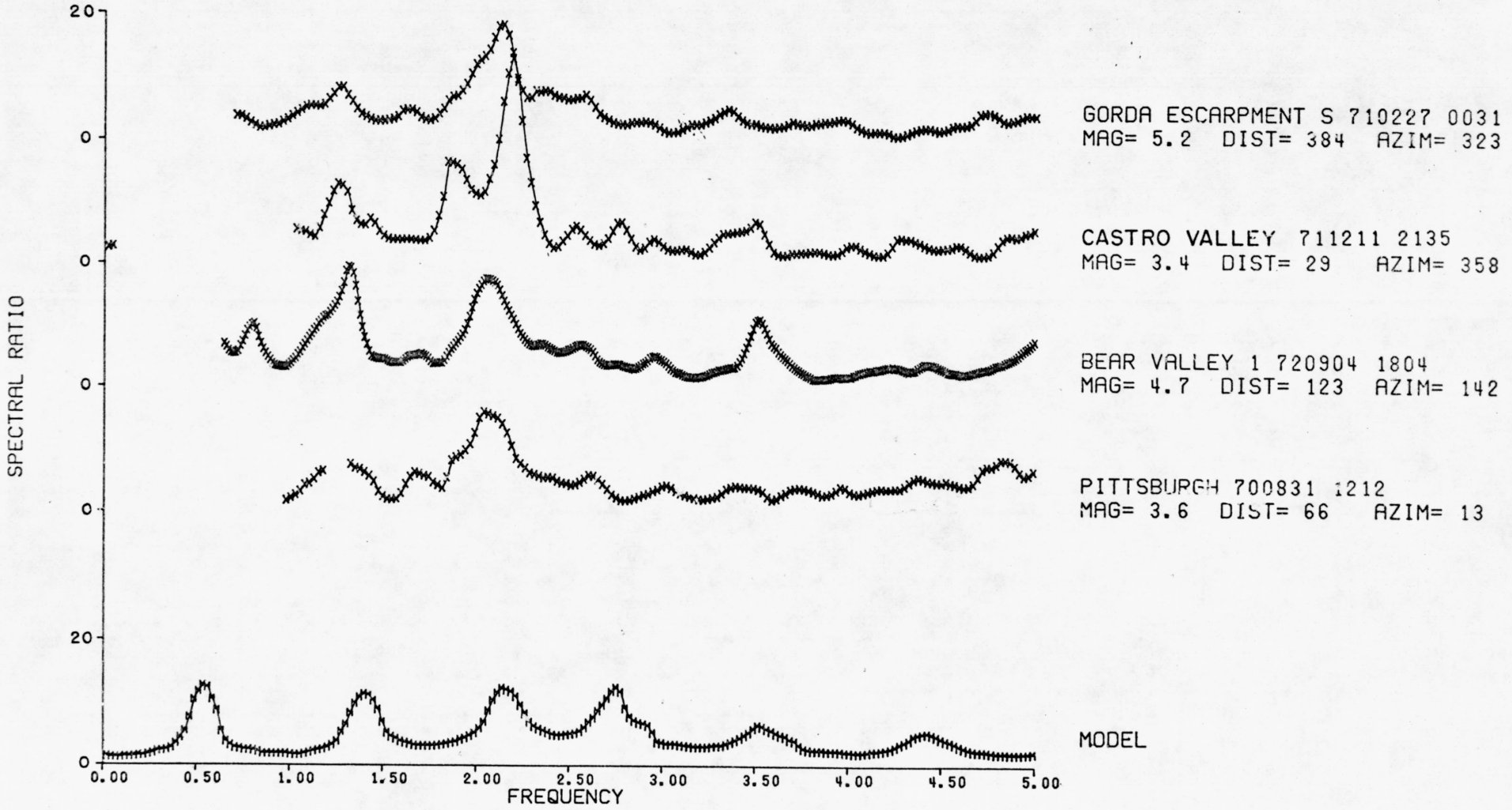
SPECTRAL RATIO
20
0
0
0
0
20
0
0.00
0.50
1.00
1.50
2.00
2.50
3.00
3.50
4.00
4.50
5.00
FREQUENCY
GORDA ESCARPMENT S 710227 0031
MAG= 5.2 DIST= 384 AZIM= 323
CASTRO VALLEY 711211 2135
MAG= 3.4 DIST= 29 AZIM= 358
BEAR VALLEY 1 720904 1804
MAG= 4.7 DIST= 123 AZIM= 142
PITTSBURGH 700831 1212
MAG= 3.6 DIST= 66 AZIM= 13
MODEL

Fig. 11

Fig. 12

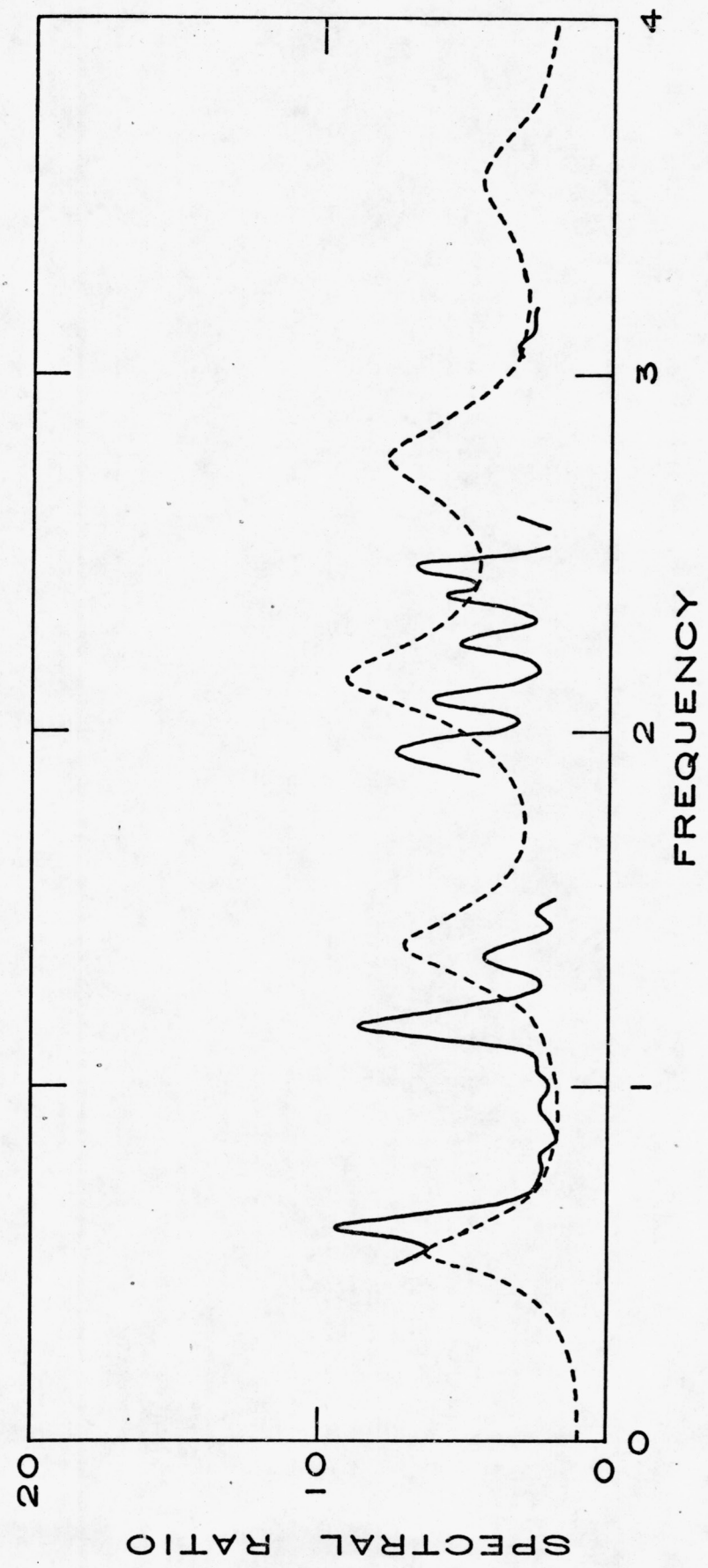

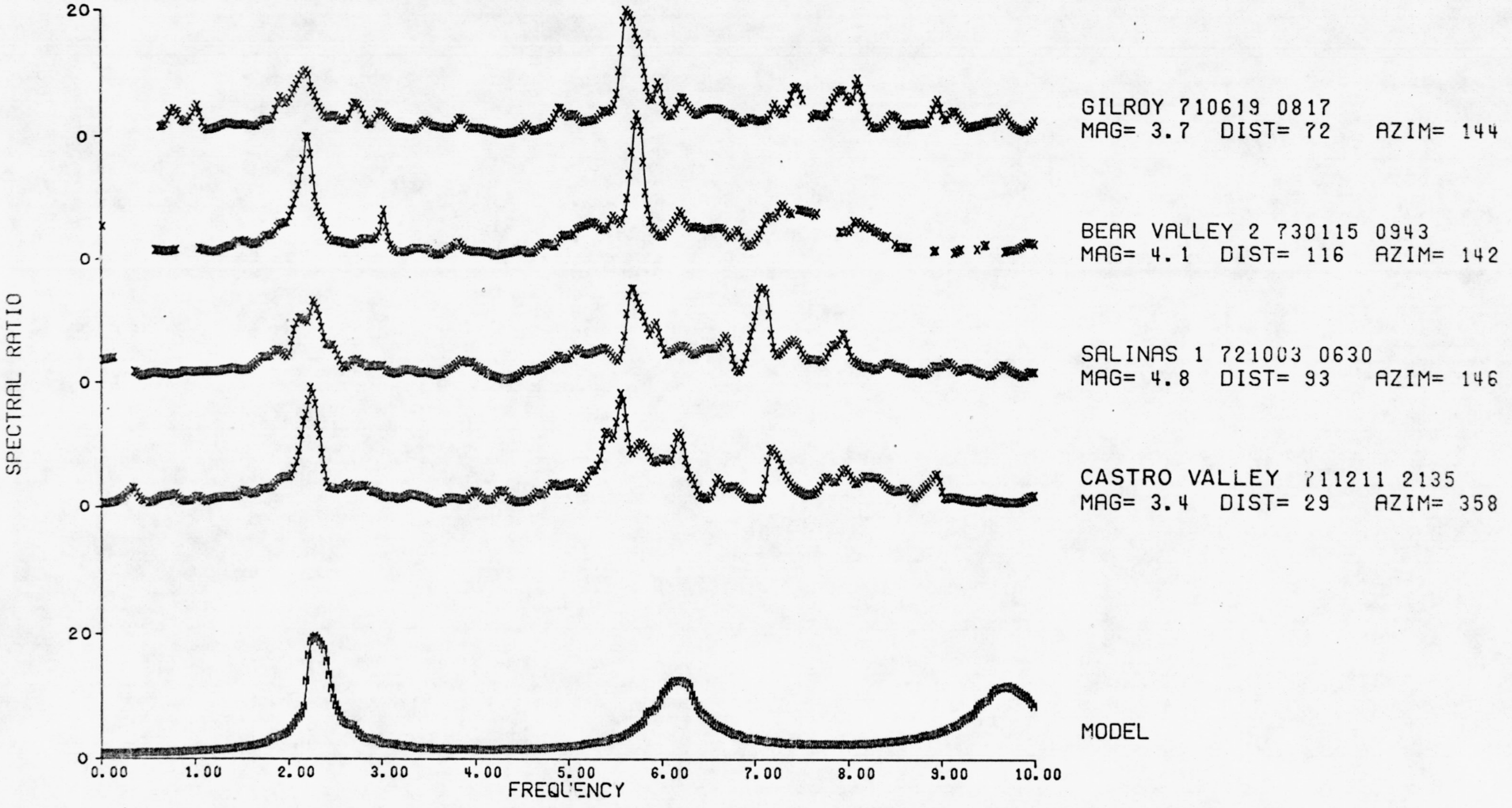
SPECTRAL RATIO
20
0
0
0
20
0
0.00
1.00
2.00
3.00
4.00
5.00
6.00
7.00
8.00
9.00
10.00
FREQUENCY
GILROY 710619 0817
MAG= 3.7 DIST= 72 AZIM= 144
BEAR VALLEY 2 730115 0943
MAG= 4.1 DIST= 116 AZIM= 142
SALINAS 1 721003 0630
MAG= 4.8 DIST= 93 AZIM= 146
CASTRO VALLEY 711211 2135
MAG= 3.4 DIST= 29 AZIM= 358
MODEL

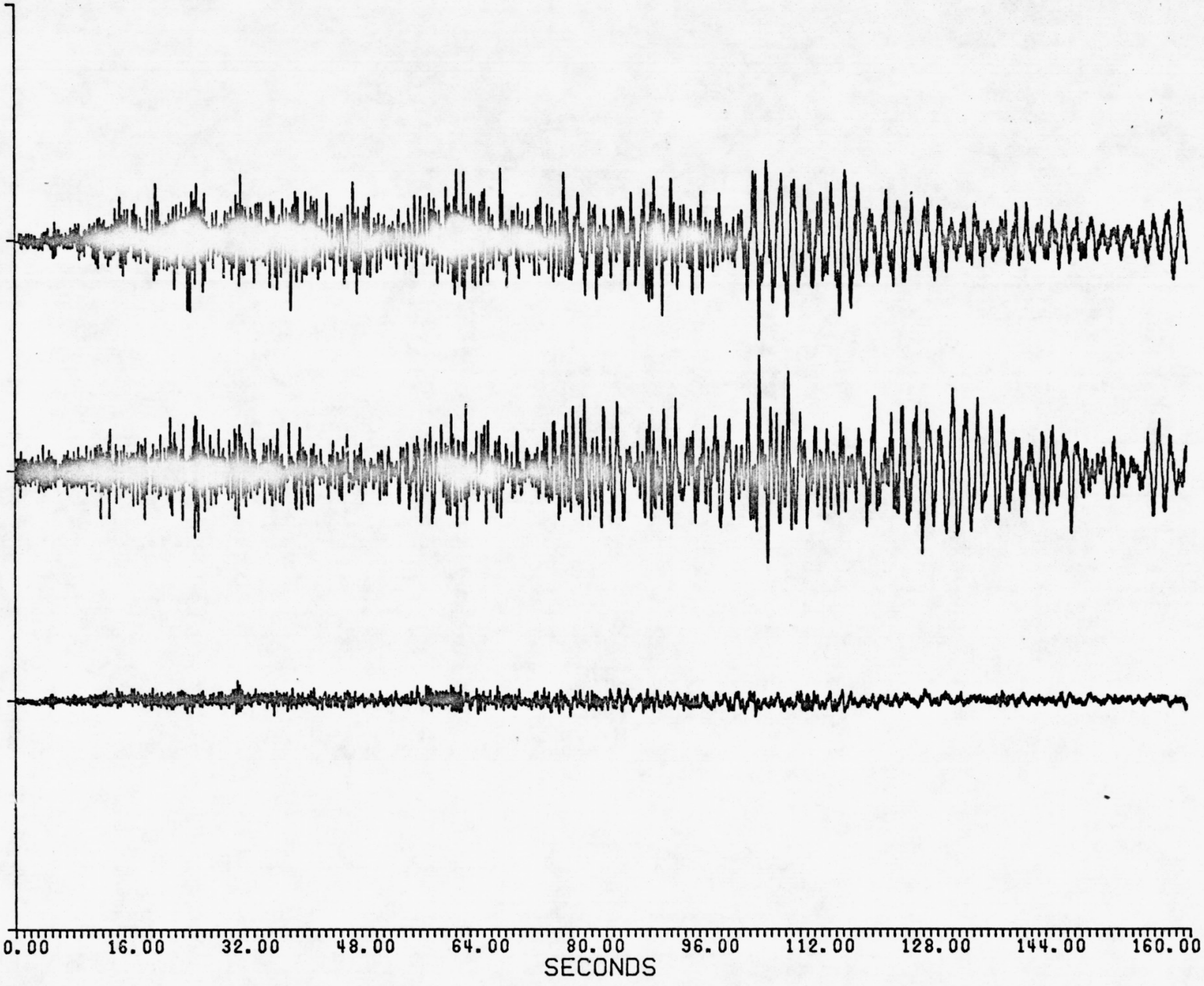
Computed
surface
Observed
surface
Observed
186 meters
0.00
16.00
32.00
48.00
64.00
80.00
96.00
112.00
128.00
144.00
160.00
SECONDS

Fig. 14

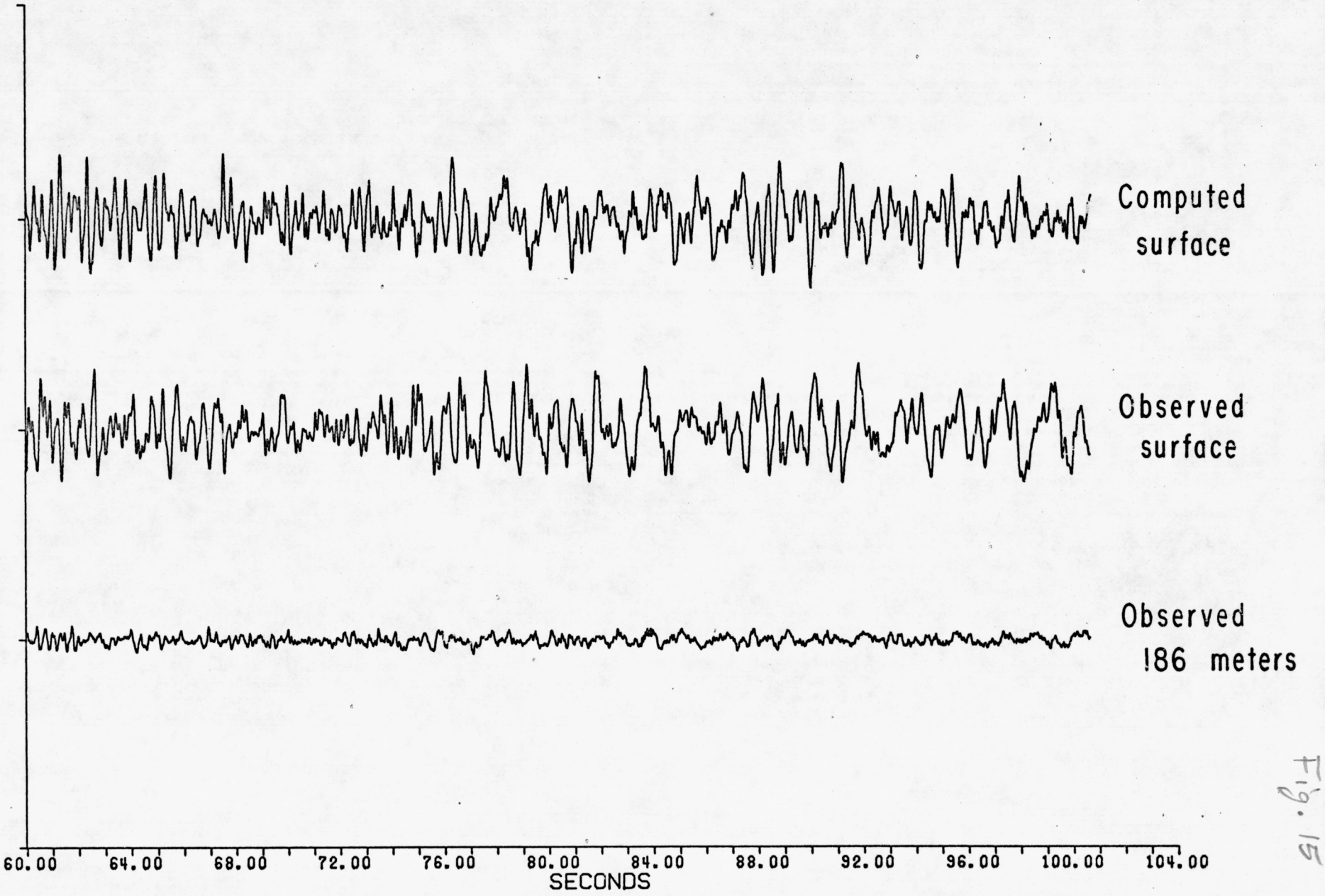
Computed
surface
Observed
surface
Observed
186 meters
60.00
64.00
68.00
72.00
76.00
80.00
84.00
88.00
92.00
96.00
100.00
104.00
SECONDS

Fig. 15

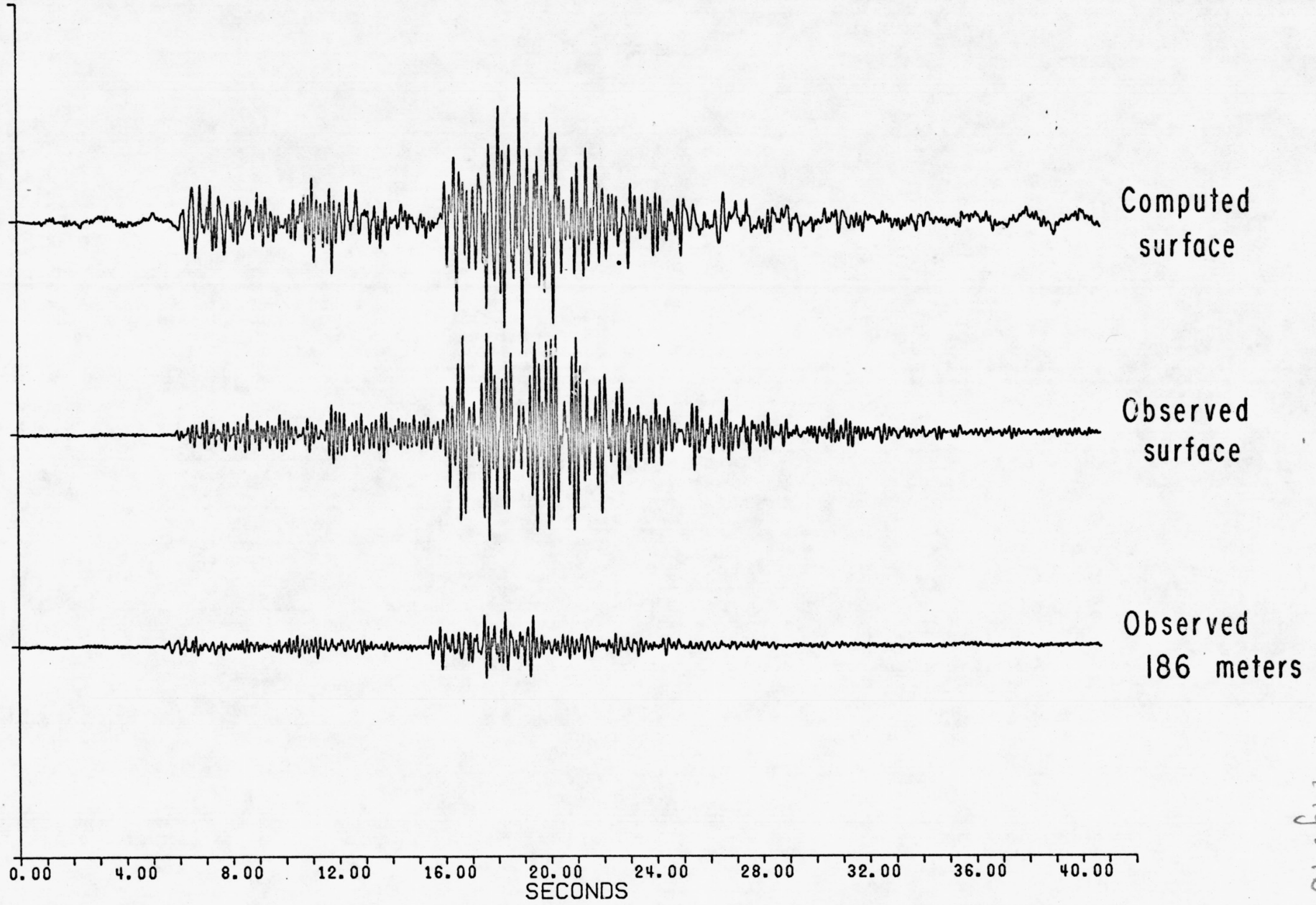
Computed
surface
Observed
surface
Observed
186 meters
0.00
4.00
8.00
12.00
16.00
20.00
24.00
28.00
32.00
36.00
40.00
SECONDS

Fig. 16

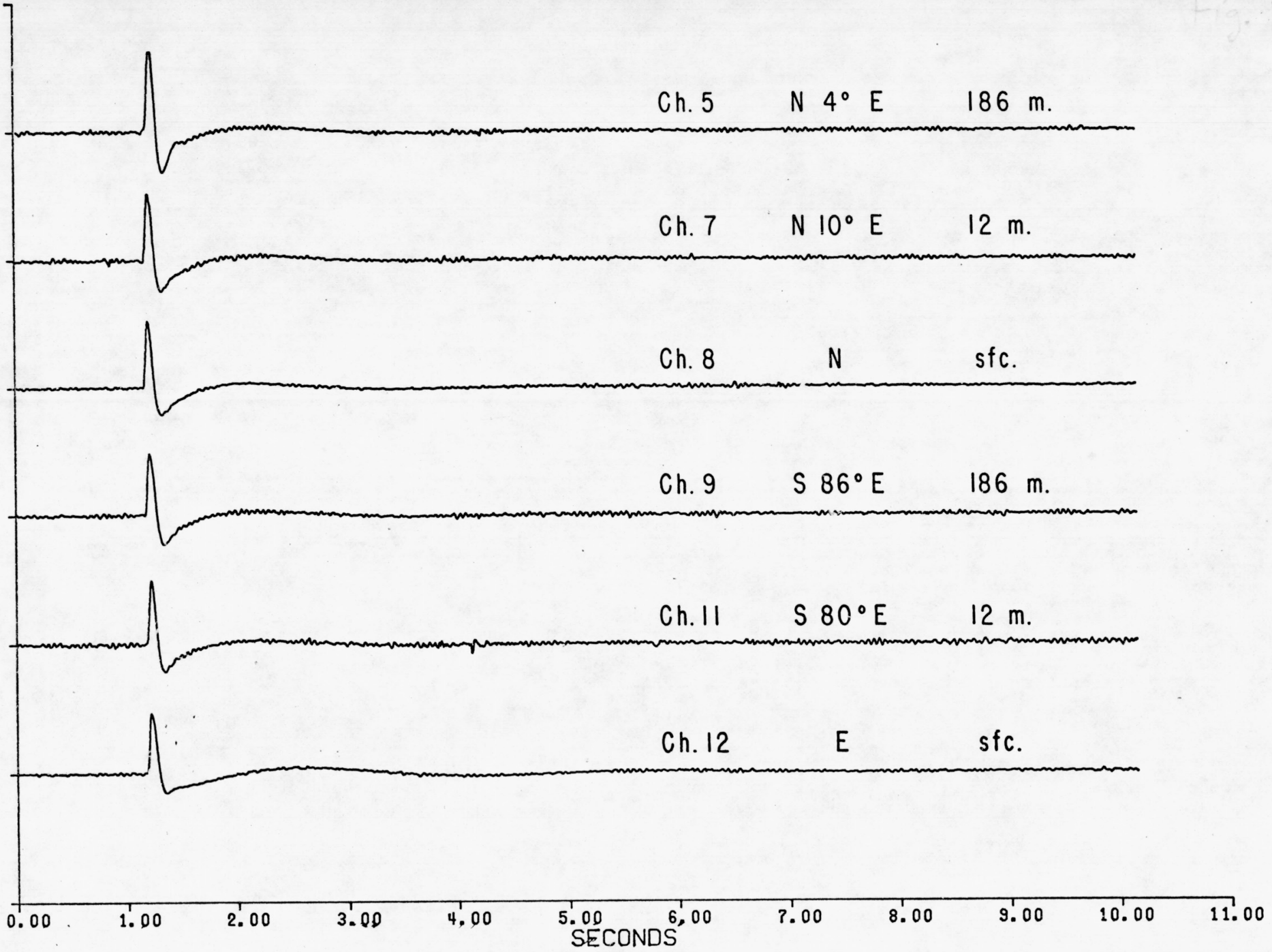
Ch. 5 N 4° E 186 m.
Ch. 7 N 10° E 12 m.
Ch. 8 N sfc.
Ch. 9 S 86° E 186 m.
Ch. 11 S 80° E 12 m.
Ch. 12 E sfc.
0.00
1.00
2.00
3.00
4.00
5.00
6.00
7.00
8.00
9.00
10.00
11.00
SECONDS

Fig. 17

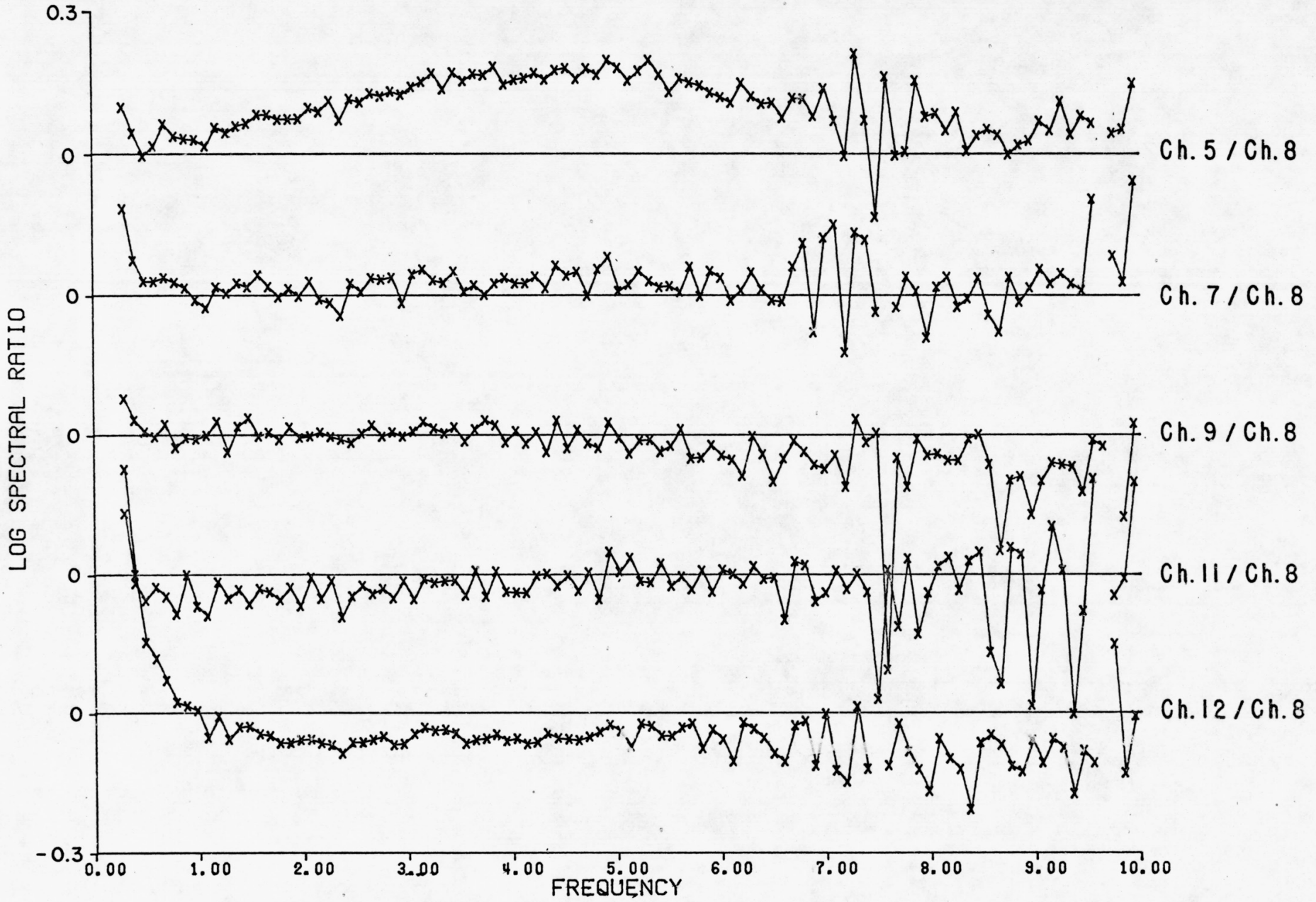
0.3
0
0
0
0
0
-0.3
LOG SPECTRAL RATIO
Ch. 5 / Ch. 8
Ch. 7 / Ch. 8
Ch. 9 / Ch. 8
Ch. 11 / Ch. 8
Ch. 12 / Ch. 8
0.00
1.00
2.00
3.00
4.00
5.00
6.00
7.00
8.00
9.00
10.00
FREQUENCY

Fig. 18

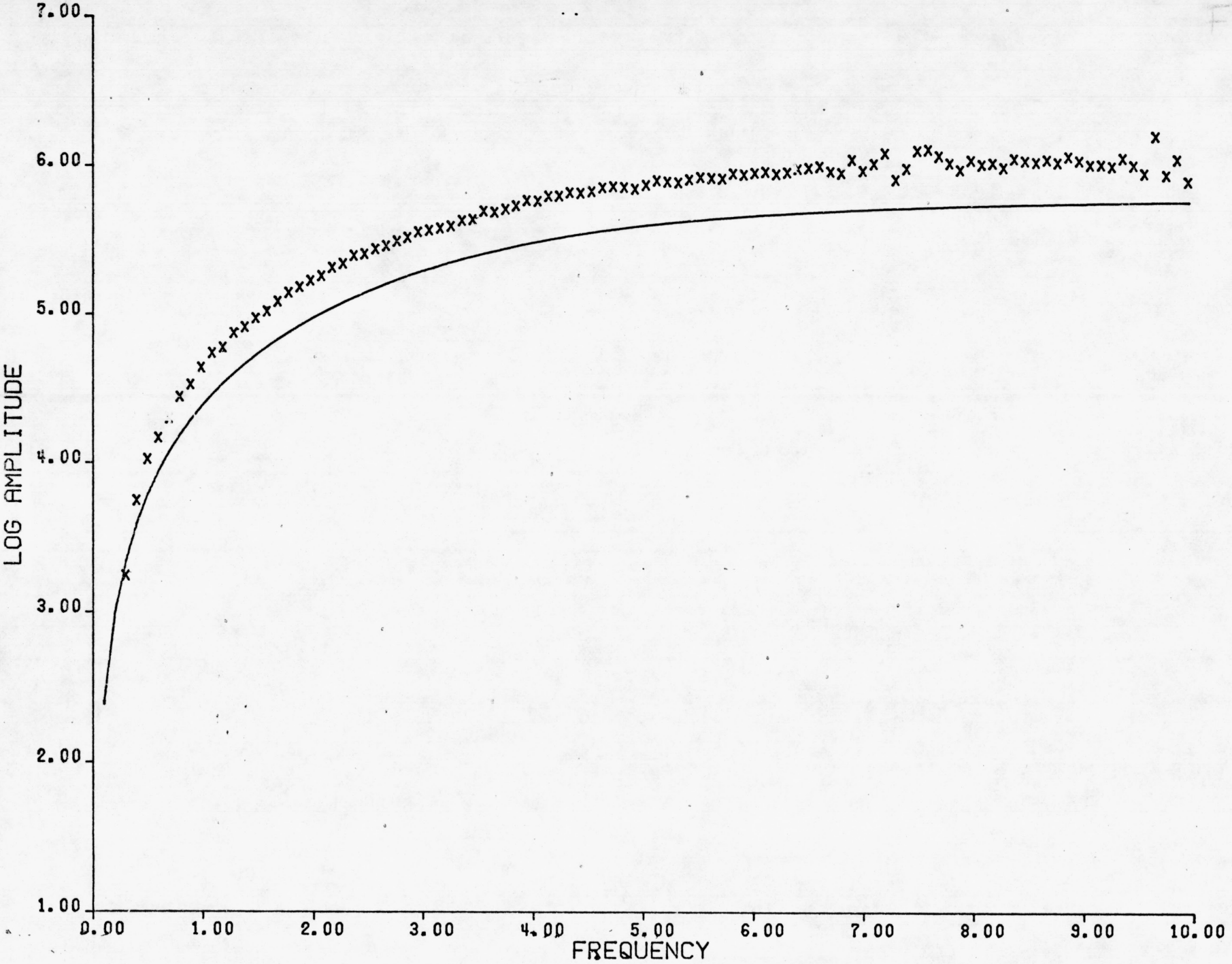
7.00
6.00
5.00
4.00
3.00
2.00
1.00
LOG AMPLITUDE
0.00
1.00
2.00
3.00
4.00
5.00
6.00
7.00
8.00
9.00
10.00
FREQUENCY

Fig. 19

Fig. 19